ISA Transactions xxx (xxxx) xxx

Contents lists available at ScienceDirect

ISA Transactions

journal homepage: www.elsevier.com/locate/isatrans

Research article

Calculation of robustly relatively stabilizing PID controllers for linear time-invariant systems with unstructured uncertainty

Radek Matušů [a,*], Bilal Senol [b], Libor Pekař [c]

[a] Centre for Security, Information and Advanced Technologies (CEBIA–Tech), Faculty of Applied Informatics, Tomas Bata University in Zlín, nám. T. G. Masaryka 5555, 760 01 Zlín, Czech Republic
[b] Department of Computer Engineering, Faculty of Engineering, Inonu University, 44280 Malatya, Turkey
[c] Department of Automation and Control Engineering, Faculty of Applied Informatics, Tomas Bata University in Zlín, nám. T. G. Masaryka 5555, 760 01 Zlín, Czech Republic

ARTICLE INFO

Article history:
Received 20 September 2021
Received in revised form 21 April 2022
Accepted 22 April 2022
Available online xxxx

Keywords:
Robust control
Robust relative stability
Robust stability
Robust performance
PID controllers
Unstructured uncertainty
H-infinity norm

ABSTRACT

This article deals with the calculation of all robustly relatively stabilizing (or robustly stabilizing as a special case) Proportional–Integral–Derivative (PID) controllers for Linear Time-Invariant (LTI) systems with unstructured uncertainty. The presented method is based on plotting the envelope that corresponds to the trios of P–I–D parameters marginally complying with given robust stability or robust relative stability condition formulated by means of the H_∞ norm. Thus, this approach enables obtaining the region of robustly stabilizing or robustly relatively stabilizing controllers in a P–I–D space. The applicability of the technique is demonstrated in the illustrative examples, in which the regions of robustly stabilizing and robustly relatively stabilizing PID controllers are obtained for a controlled plant model with unstructured multiplicative uncertainty and unstructured additive uncertainty. Moreover, the method is also verified on the real laboratory model of a hot-air tunnel, for which two representative controllers from the robust relative stability region are selected and implemented.

1. Introduction

Despite the existence of a wide variety of sophisticated control approaches, the Proportional–Integral–Derivative (PID) controllers still play a fundamental role in a great majority of real control engineering applications even nowadays [1–3]. The unshakeable position of PID controllers was also confirmed by the survey published in the IEEE Control Systems Magazine in 2017 [4], where industry-aware control experts were asked about their perceptions of the industry impact/success of a dozen of advanced control technologies. The PID control was also included for calibration purposes [4]; however, quite surprisingly (or actually not?), it routed all advanced approaches, as the experts unanimously ranked the PID control at the top of control technologies having high industry impact. Therefore, it is still worth researching the PID-based control loops, especially from the viewpoint of their robustness [4–7], in order to make these simple and easily implementable control algorithms applicable to systems under various conditions of uncertainty.

Remind that linear robust control methods usually start from an uncertain Linear Time-Invariant (LTI) model of the controlled plant. The uncertainty, which is incorporated into the model, can be considered as a cost for keeping the relative simplicity of an LTI model even for the systems with much more complicated (even nonlinear) behavior, the imprecise physical properties knowledge, or the parameters (“slowly”) depending on changing conditions.

There are three principal approaches to modeling the uncertainty for the purpose of robust control, namely parametric uncertainty [8–11], unstructured uncertainty [9,12–16], and Linear Fractional Transformation (LFT) [13,17–20].

The first, and probably the most natural and comprehensible, approach uses so-called parametric uncertainty [8–11]. The construction of the models with parametric uncertainty works on the assumption that the structure of the system, i.e., its order, is fixed and known, but the real physical parameters are known only imprecisely. Most frequently, the uncertain parameters are bounded by the real intervals, but other types of bounds are also possible. Moreover, the systems with parametric uncertainty may have various uncertainty structures, which specify their complexity. However, as stated in [21], sometimes it is not possible or practical to represent the uncertainty by means of the parametric approach, and thus other models may be utilized.

The second mentioned description, based on the unstructured uncertainty, uses the restriction of the spread of the frequency

* Corresponding author.
E-mail address: rmatusu@utb.cz (R. Matušů).

https://doi.org/10.1016/j.isatra.2022.04.037
0019-0578/

characteristics. Thanks to this, it does not even need, contrary to the parametric uncertainty, any knowledge of the system structure. There are several types of unstructured uncertainty available, as will be named in the following Section 2 [9,12–16].

Finally, a general control configuration that leads to the description of a control system by means of LFT represents the third option. This universal approach allows the formulation of many linear control problems using an array of methods (e.g., Linear Quadratic Gaussian (LQG), H_2, H_∞ or μ control), and it is especially advantageous for Multiple-Input Multiple-Output (MIMO) systems [13,17–20].

This paper utilizes the models with the unstructured uncertainty, as a favorable compromise among description simplicity, ability to cover even the systems with unknown structure (order), and the efficacy for control design methods, especially for Single-Input Single-Output (SISO) systems. Therefore, the key motivation for utilizing the unstructured uncertainty approach in modeling the uncertainty can be seen in a possibility to include not only parameter variations but also various unmodeled dynamics including nonlinear, high-order, or other complex behavior into a relatively simple uncertainty model that is combined with a nominal LTI model. Nevertheless, in the illustrative examples, the models with unstructured uncertainty are constructed just on the basis of the original models with parametric uncertainty because of simplicity. Besides, the unstructured uncertainty models are advantageous for H_∞ norm-based control design techniques. A comparison of the (fractional-order) models with parametric uncertainty, unstructured multiplicative uncertainty, and unstructured additive uncertainty, as well as the corresponding approaches to the robust stability investigation, were presented in [22].

Many applications of robust control approaches, especially those based on the H_∞ tools, using models with unstructured uncertainty can be found in the literature. For example, [23] presented a synthesis of a robust controller via a pole placement method and H_∞ metrics, and it utilized the technique for control of a servomechanism, modeled by means of the unstructured uncertainty. Recently, [24] solved a robust control synthesis for wave energy converters under unstructured uncertainty as an LQG problem with an associated H_∞ constraint. Further, [25] applied a methodology using H_∞ optimization, Linear Matrix Inequalities (LMIs), and unstructured uncertainty to design robust controllers for a two-input two-output temperature system.

However, the application of H_∞ norm-based techniques in control synthesis usually leads to high-order and thus impractical controllers [21]. Despite the efforts to put constraints on the order of H_∞ controllers [26–28], many of these methods represent relatively difficult computational problems. Due to the extreme popularity and extensive use of PID controllers, several works naturally focused on synthesizing H_∞ PID controllers. For example, [29] presented a design of H_∞ PID controllers based on a generalization of the Hermite–Biehler Theorem and linear programming. Then, the use of H_∞ approximation for the online adaptation of PID controller parameters was discussed in [30]. More recently, [31] offered a constructive determination of the set of stabilizing PI and PID controllers attaining an H_∞ norm bound on the error transfer function and developed a relationship between this H_∞ norm specification and guaranteed classical gain and phase margins.

It is understandable that an array of researchers have focused on the robustness of these conventional PID (and PI as a special case) control loops also specifically under unstructured uncertainty. For example, the idea of plotting the contour graph of H_∞ norm of weighted complementary sensitivity for robustly stabilizing PI controllers and plants with unstructured uncertainty was shown in [14]. Subsequently, the same model of a paper bleaching process as in [14] was also used in [16] for the purpose of the comparison of parametric uncertainty-based and unstructured uncertainty-based approaches to uncertainty modeling and robust stability analysis. Moreover, the idea from [14] was applied to finding the robustly stabilizing PI controllers via plotting the boundary contour in a P-I plane for systems with unstructured multiplicative [32] or unstructured additive [33] uncertainty. Then, an analytically based procedure for designing low-order controllers that satisfy frequency-dependent sensitivity specifications for SISO plants with unstructured uncertainty was presented in [34]. A small gain theorem-based technique for designing robust PI/PID controllers for systems described by the unstructured uncertainty model was discussed in [35] and afterward in [36]. A computationally favorable method for calculation of all H_∞ robustly stabilizing P controllers (gains) for SISO LTI systems affected by unstructured multiplicative uncertainty was proposed in [21]. Later, a method, based on the system's frequency response, for finding all PID controllers satisfying a robust performance constraint for a given SISO transfer function with time delay was introduced in [37]. Further, the paper [38] provided a set of simulation results for robust PID control of a hydraulic system with unstructured uncertainty. Recently, in [39], a robust PI controller was designed for a textile-reinforced composite integrated with shape memory actuators, modeled by means of an unstructured uncertainty approach.

Besides the unstructured uncertainties, the design of conventional PI or PID controllers for plants with parametric uncertainty represents its own popular and frequently researched field with many interesting works, which will not be cited here. The interested reader can find a relevant literature review in [40]. However, even for the purposes of this paper, it is worth mentioning at least several H_∞-based methods, such as these presented in [41–43]. Furthermore, a mixture of structured and unstructured uncertainties was discussed, e.g., in [44,45] for PID controllers, and in [46,47] for more general higher-order controllers.

Some works extended the concept of (absolute) stability to relative stability [48–51], which also gives a certain degree of stability, i.e., it says how close the system is to instability. Since the shifted half-plane ensures a specified settling time of the response [51], the relative stability can be considered as a tool for obtaining some level of performance as well. Moreover, the relative stability can be further extended to so-called robust relative stability [52–54] in the same way as from the (absolute) stability to the robust stability. Thus, it means that the prescribed relative stability has to be ensured not only for a nominal plant but for all possible members of an uncertain family, so even for the worst case.

This paper aims at the calculation of all robustly stabilizing or robustly relatively stabilizing PID controllers for LTI systems with unstructured uncertainty. The presented graphical approach is based on obtaining the envelope that corresponds to the trios of P–I–D parameters that marginally fulfill given robust stability or robust relative stability condition formulated by means of the H_∞ norm. The practical solution is done by a numerical procedure with some given tolerance to the applied condition, and a set of P-I contours is obtained for some sampled fixed values of D parameters, which consequently forms the whole envelope. Thus, this method allows calculating the region of robustly stabilizing or robustly relatively stabilizing PID controllers in a P–I–D space. In the previous works, the idea of finding the robust stability area through plotting the boundary contour in a P-I plane was used for systems with multiplicative [14,32] and additive [33] uncertainty, but only for PI controllers and only from the robust (absolute) stability viewpoint. On the other hand, this paper enriches the method and presents the calculation of robustly relatively stabilizing (or robustly stabilizing as a special case) PID

controllers. In other words, the key contribution of this work consists in the extension of the method for PID controllers and its generalization for the concept of robust relative stability. In order to show the technique's applicability, the illustrative examples are elaborated, in which the regions or robustly stabilizing PID controllers and robustly relatively stabilizing PID controllers are calculated for the controlled plant models with unstructured multiplicative or unstructured additive uncertainty. Furthermore, the practical applicability of the technique is also demonstrated by means of real experiments on the laboratory model of a hot-air tunnel. The process of airflow speed in this tunnel is modeled as the system with unstructured multiplicative uncertainty, and the region of robustly relatively stabilizing PID controllers is obtained. Subsequently, two representative controllers are selected from this region and tested to control the speed of airflow in the hot-air apparatus.

Thus, the main contribution of this paper and the benefits of the presented method can be summarized as follows:

- A technique for calculating all robustly relatively stabilizing PID controllers with some given robust stability margin α (typically $\alpha > 1$) for LTI plants with unstructured uncertainty is introduced.
- The core of the method is based on obtaining the envelope determined by the trios of P–I–D parameters that marginally comply with a given robust relative stability condition formulated via the H_∞ norm.
- The current work represents the extension of the previous works, where only PI controllers were considered and only from the robust (absolute) stability viewpoint.
- Thanks to the unstructured uncertainty, the structure (order) of the controlled system is needles to know, and thus not only parameter variations but also various unmodeled complicated dynamics may be covered in the model.
- All common types of unstructured uncertainty may be used in the method. The choice will influence the form of the applied robust relative stability condition.
- Robustly (absolutely) stable PID controllers can be obtained as a special case (for $\alpha = 1$) of the robustly relatively stable PID controllers.
- In the illustrative examples, the two most frequent kinds of unstructured uncertainty models, that is, multiplicative and additive, are discussed.
- The practical applicability of the method is verified via the real control experiments on the laboratory model of a hot-air tunnel.

The remainder of this article is structured as follows. The models with unstructured uncertainty, their classification, and mathematical description are reminded in Section 2. Then, an overview of (classic) robust stability conditions and (classic) robust performance conditions for systems under unstructured uncertainty are summarized in Sections 3 and 4, respectively. The main contribution of the article resides in Section 5, where an approach for calculating robust (namely robustly stabilizing and robustly relatively stabilizing) controllers is presented. Further, the specific illustrative example for a plant with unstructured multiplicative uncertainty is elaborated and discussed in Section 6. Then, a similar synthesis and discussion, but for the plant model with unstructured additive uncertainty, is provided in Section 7. Subsequently, the real control experiments on the laboratory model of a hot-air tunnel are presented in Section 8. The final Section 9 offers some concluding remarks.

2. Systems with unstructured uncertainty

Since the idea of robust control is based on respecting the discrepancy between the actual behavior of the real-life controlled plant and the idealized behavior of its mathematical model by means of introducing the uncertainty into this model, the construction of such models with uncertainty represents the essential task. As mentioned above, three main approaches to modeling the uncertainty for robust control are typically utilized — parametric uncertainty, unstructured uncertainty, and LFT. From these options, the unstructured uncertainty-based approach seems to represent an advantageous trade-off between simplicity and effectiveness. Firstly, it is not necessary to know the true structure (order) of the controlled plant. Consequently, not only parameter changes but also various unmodeled complex dynamics may be covered by the unstructured uncertainty model. However, secondly, the final plant model still remains simple enough (LTI), and it is convenient for control design methods, especially those based on H_∞ techniques.

The various kinds of unstructured uncertainty models can be further classified as follows [13]:

- Multiplicative uncertainty
- Additive uncertainty
- Inverse multiplicative uncertainty
- Inverse additive uncertainty.

Besides, the multiplicative uncertainty and the inverse multiplicative uncertainty may have their input and output forms for the general case of MIMO systems. However, for SISO systems (that are considered in this paper), the input and output forms are equivalent.

The multiplicative uncertainty is probably the most commonly utilized type of unstructured uncertainty in control engineering. A possible reason can be seen in the fact that its numerical value is more informative than in the case of additive uncertainty [13]. The perturbed model $G_M(s)$ with the (input) multiplicative uncertainty can be described by the transfer function:

$$G_M(s) = [1 + W_M(s)\Delta_M(s)]\, G_0(s), \tag{1}$$

where $G_0(s)$ represents a nominal model, $W_M(s)$ is a weight function (typically stable and minimum-phase one) representing uncertainty dynamics (in other words, it expresses how the maximum uncertainty magnitude is distributed over the frequency), and $\Delta_M(s)$ means the uncertainty itself, that is, the uncertain information on the true magnitude and phase of perturbation. This (allowable) uncertainty is any stable function that complies with the inequality:

$$\|\Delta_M(s)\|_\infty \le 1 \Rightarrow |\Delta_M(j\omega)| \le 1 \quad \forall\omega. \tag{2}$$

Alternatively, it is possible to replace the condition of the stability of $\Delta_M(s)$ by the prerequisite for the same amount of right-hand (unstable) poles for all members of the family, i.e., the same amount of right-hand poles of $G_0(s)$ and $G_M(s)$ for all $\Delta_M(s)$. Nevertheless, the requirement of stable $\Delta_M(s)$ is preferred [13].

The diagram of the system with multiplicative uncertainty (1) is shown in Fig. 1, where u stands for the input and y for the output signal of the perturbed plant.

The weight function $W_M(s)$ has to be selected to fulfill the inequality:

$$\left|\frac{G_M(j\omega)}{G_0(j\omega)} - 1\right| \le |W_M(j\omega)| \quad \forall\omega, \tag{3}$$

which means that $W_M(s)$ must cover the normalized perturbations (relative errors) from above for all frequencies.

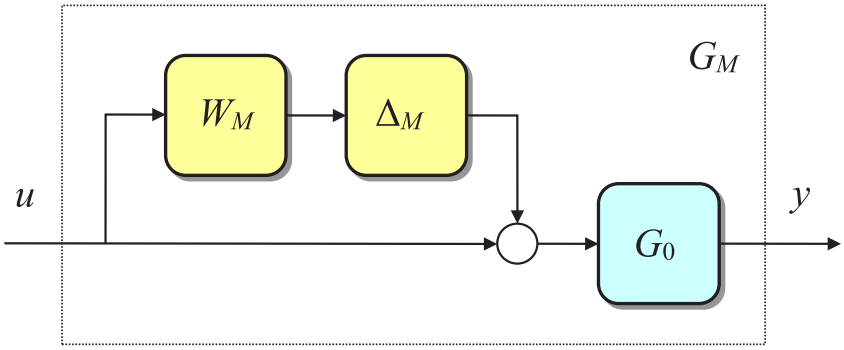

Fig. 1. System with (input) multiplicative uncertainty (1).

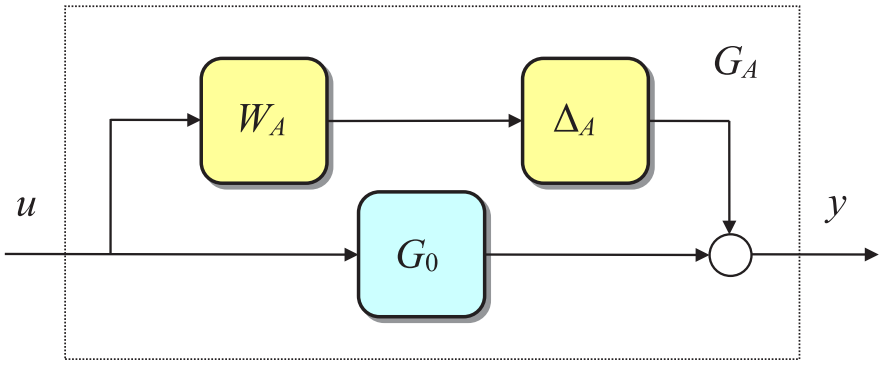

Fig. 2. System with additive uncertainty (4).

The additive uncertainty is another popular class of unstructured uncertainty models. The system with additive uncertainty is given by:

$$G_A(s) = [1 + W_A(s)\Delta_A(s)]\, G_0(s), \tag{4}$$

where the meaning of $G_0(s)$, $W_A(s)$, and $\Delta_M(s)$ is analogous as in the previous multiplicative uncertainty case (1). A graphical representation of the system with additive uncertainty can be seen in Fig. 2.

The choice of the weight function $W_A(s)$ has to be in accordance with the inequality:

$$|G_A(j\omega) - G_0(j\omega)| \le |W_A(j\omega)| \quad \forall\omega. \tag{5}$$

Please note that the multiplicative uncertainty models and the additive uncertainty models are equivalent if [13]:

$$|W_A(j\omega)| = |G_0(j\omega)| \cdot |W_M(j\omega)| \quad \forall\omega. \tag{6}$$

For the sake of completeness, the systems with the (input) inverse multiplicative uncertainty and the inverse additive uncertainty are defined as, respectively:

$$G_{IM}(s) = [1 - W_{IM}(s)\Delta_{IM}(s)]^{-1}\, G_0(s), \tag{7}$$

$$G_{IA}(s) = G_0(s)\,[1 - W_{IA}(s)\Delta_{IA}(s)G_0(s)]^{-1}. \tag{8}$$

Then, Figs. 3 and 4 show the corresponding diagrams.

3. (Classic) robust stability conditions

Assume an open-loop system with the transfer function:

$$L_0(s) = C(s)G_0(s), \tag{9}$$

where $C(s)$ is a controller and $G_0(s)$ stands for a nominal plant. Then, a sensitivity function and a complementary sensitivity function can be expressed as, respectively:

$$S_0(s) = \frac{1}{1 + L_0(s)}, \tag{10}$$

$$T_0(s) = \frac{L_0(s)}{1 + L_0(s)}. \tag{11}$$

First, consider that the controlled plant is affected by multiplicative uncertainty. Provided that a nominal closed-loop control system (i.e., for $G_0(s)$) is stable, the corresponding perturbed closed-loop control system is robustly stable if and only if [12,13]:

$$\|W_M(s)T_0(s)\|_\infty < 1, \tag{12}$$

which can also be formulated as an upper bound restriction on the complementary sensitivity function as:

$$|T_0(j\omega)| < \frac{1}{|W_M(j\omega)|} \quad \forall\omega. \tag{13}$$

The basic condition (12) can be rewritten in the following form:

$$\left|\frac{W_M(j\omega)L_0(j\omega)}{1 + L_0(j\omega)}\right| < 1 \quad \forall\omega \Rightarrow |W_M(j\omega)L_0(j\omega)| < |L_0(j\omega) - (-1)| \quad \forall\omega, \tag{14}$$

which may be nicely graphically interpreted, as shown in Fig. 5.

For the sake of simplicity, Fig. 5 supposes that the Nyquist plot of a stable (integrators are considered as stable systems here) open-loop transfer function $L_0(s)$ is presented. Then, evidently, Fig. 5 depicts that the nominally stable closed-loop system is also robustly stable if and only if the critical point $[-1, 0j]$ is

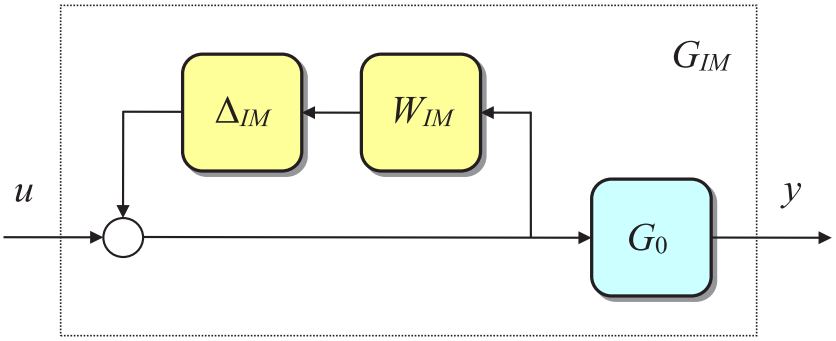

Fig. 3. System with (input) inverse multiplicative uncertainty (7).

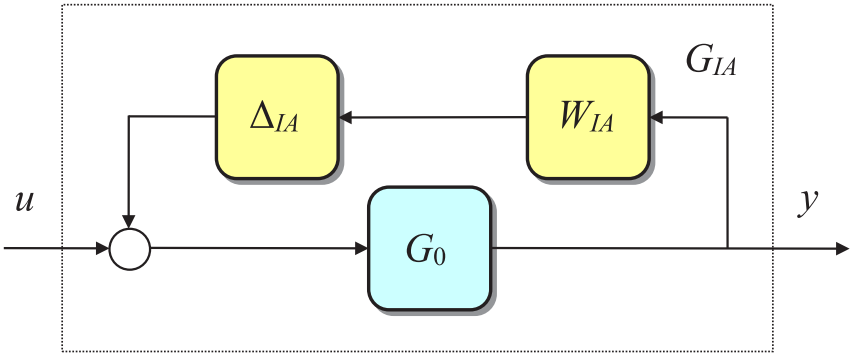

Fig. 4. System with inverse additive uncertainty (8).

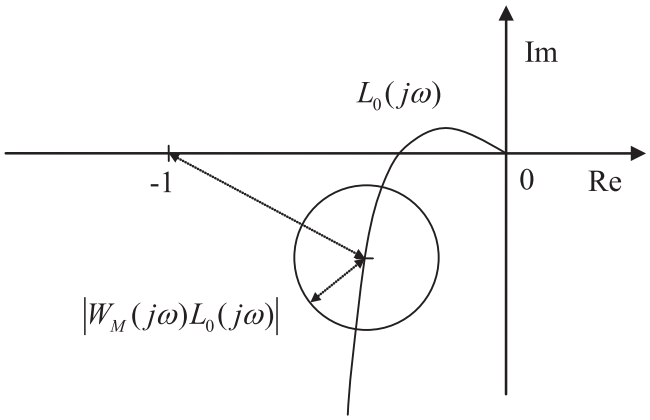

Fig. 5. Graphical interpretation of the condition of robust stability under multiplicative uncertainty [15].

excluded from the envelope of Nyquist curves with a radius of $|W_M(j\omega)L_0(j\omega)|$ and the center $L_0(j\omega)$.

The analogous robust stability conditions can also be derived for the other types of unstructured uncertainty models. They are as follows [12]:

$$\|W_A(s)C(s)S_0(s)\|_\infty < 1, \tag{15}$$

$$\|W_{IM}(s)G_0(s)S_0(s)\|_\infty < 1, \tag{16}$$

$$\|W_{IA}(s)S_0(s)\|_\infty < 1, \tag{17}$$

and they are valid for additive (4), inverse multiplicative (7), and inverse additive (8) uncertainty models, respectively.

4. (Classic) robust performance conditions

Recall that the condition for the nominal performance of a closed-loop system (without perturbations), expressed in terms of weighted sensitivity, is [12,13]:

$$\|W_P(s)S_0(s)\|_\infty = \|W_P(s)S(s)\|_\infty < 1, \tag{18}$$

where $W_P(s)$ is a (performance) weight chosen by the designer. The condition (18) can be graphically illustrated by means of the Nyquist plot of open-loop transfer function $L(s)$ (usually stable one for simplicity), which must remain outside a disc of radius $|W_P(j\omega)|$ with the center on $[-1, 0j]$.

Under the assumption of the perturbed plant, one may be interested in robust performance, i.e., not only stability but also some specified performance must hold for all possible members in the plant family (such as $G_M(s)$).

In the multiplicative uncertainty case (1), a necessary and sufficient condition for robust performance is [12,13]:

$$\||W_P(s)S_0(s)| + |W_M(s)T_0(s)|\|_\infty < 1. \tag{19}$$

The basic condition (19) can be easily modified to the form:

$$|W_P(j\omega)| + |W_M(j\omega)L_0(j\omega)| < |L_0(j\omega) - (-1)| \quad \forall\omega, \tag{20}$$

which leads to the nice graphical interpretation, as depicted in Fig. 6.

According to Fig. 6, the robustly stable closed-loop system is also robustly performing if and only if a disc of radius $|W_P(j\omega)|$ with the center on the critical point $[-1, 0j]$ is not included in the envelope of Nyquist plots with a radius of $|W_M(j\omega)L_0(j\omega)|$ and the center $L_0(j\omega)$.

The direct application of the condition (19) for controller design is unsuitable because such defined robust performance control design problem cannot be solved [12,55]. Thus, other approaches have to be used. For example, the condition (19) may be relatively closely approximated (within a factor of at most $\sqrt{2}$)

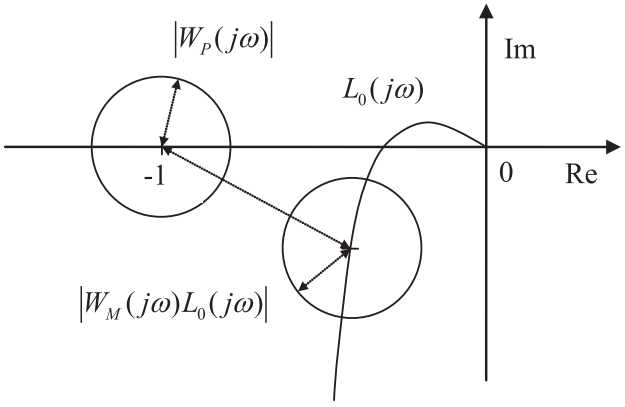

Fig. 6. Graphical interpretation of the condition of robust performance under multiplicative uncertainty.

for the purpose of controller design for SISO systems by so-called mixed sensitivity H_∞ condition:

$$\left\| \begin{matrix} W_P(s)S_0(s) \\ W_M(s)T_0(s) \end{matrix} \right\|_\infty = \sup_{\omega\in\mathbb{R}} \sqrt{|W_P(j\omega)S_0(j\omega)|^2 + |W_M(j\omega)T_0(j\omega)|^2} < 1. \quad (21)$$

Again, for the sake of fullness, the overview of the robust performance conditions also for the additive (4), inverse multiplicative (7), and inverse additive (8) uncertainty models are as follows, respectively [12]:

$$\| |W_P(s)S_0(s)| + |W_A(s)C(s)S_0(s)| \|_\infty < 1, \quad (22)$$

$$\| |W_P(s)T_0(s)| + |W_{IM}(s)G_0(s)S_0(s)| \|_\infty < 1, \quad (23)$$

$$\| |W_P(s)T_0(s)| + |W_{IA}(s)S_0(s)| \|_\infty < 1, \quad (24)$$

while the conditions (23) and (24) suppose that the nominal performance condition has not the standard form (18), but it is given by the formula [12]:

$$\|W_P(s)T_0(s)\|_\infty = \|W_P(s)T(s)\|_\infty < 1. \quad (25)$$

5. Calculation of robust PID controllers

The aim of this section is to present a graphical approach to calculating robust (more specifically, robustly stabilizing or robustly relatively stabilizing) PID controllers for LTI plants with unstructured uncertainty. The main idea is based on plotting the envelope that corresponds to the trios of P–I–D parameters marginally complying with given robust stability or robust relative stability condition. Practically, a set of P-I contours is obtained (under an accepted tolerance of an applied condition) for some sampled fixed values of D parameters, which shapes the whole envelope. Thus, this procedure enables obtaining the region of robustly stabilizing or robustly relatively stabilizing PID controllers in a P–I–D space.

Previously, the idea of finding the robust stability area by means of plotting the boundary contour in a P-I plane was used for systems with multiplicative [14,32] and additive [33] uncertainty, but only for PI controllers and only from the perspective of the pure robust (absolute) stability. This paper extends the approach and presents the calculation of robustly stabilizing or robustly relatively stabilizing PID controllers.

5.1. Robustly stabilizing controllers

The controller $C(s)$ that guarantees robust stability has to be designed in order to meet the basic condition, which is the inequality (12), (15), (16) or (17), depending on the kind of the unstructured uncertainty model. Thus, under the assumption of PID controllers, the region of robustly stabilizing parameters can be depicted in the P–I–D space by means of the robust stability border P–I–D trios, that is, the triplets of P–I–D parameters that fulfill one of the conditions:

$$\|W_M(s)T_0(s)\|_\infty = 1, \quad (26)$$

$$\|W_A(s)C(s)S_0(s)\|_\infty = 1, \quad (27)$$

$$\|W_{IM}(s)G_0(s)S_0(s)\|_\infty = 1, \quad (28)$$

$$\|W_{IA}(s)S_0(s)\|_\infty = 1, \quad (29)$$

where the first Eq. (26) will be used for the multiplicative uncertainty (1), the second condition (27) for the additive uncertainty (4), the third version (28) for the inverse multiplicative uncertainty (7), and the last Eq. (29) for the inverse additive uncertainty (8).

Anyway, the P–I–D trios meeting the corresponding condition define the surface that divides the P–I–D space into robustly stabilizing and robustly non-stabilizing regions. Consequently, the final set of robustly stabilizing controllers can be determined.

5.2. Robustly relatively stabilizing controllers

In accordance with the previous Section 4, the controller $C(s)$ that ensures the robust performance has to comply with one of the conditions (19), (22), (23) or (24), depending on the kind of the unstructured uncertainty. It was also mentioned that these basic conditions are usually, for the sake of controller design, approximated by a reasonable compromise robust performance measure (mixed sensitivity H_∞ condition), such as the modified condition (21) for the multiplicative uncertainty model. Although it seems the graphical approach described in the previous Section 5.1 should be generally applicable also to robust performance conditions (19), (22), (23) or (24) (since the conditions would be used "just" for a set of robust performance boundary tests, and not for designing the controller in fact), the necessary calculations would be still quite demanding. Thus, this paper prefers another approach, and instead of using the classic robust performance conditions (or their compromise approximations), it presents the robust relative stability-based method. In other words, no robustly performing controllers in the sense of conditions (19), (22), (23) or (24) are designed, but rather the controllers that guarantee robust stability with some predetermined safety margin (robust relative stability), which, as a result, leads to some robust performance level as well.

This idea will be further explained through the following elaboration for the multiplicative uncertainty model: The graphical representation of classic robust performance condition (19) was depicted in Fig. 6. It can be seen that the forbidden neighborhood of the critical point $[-1, 0j]$ for the envelope of Nyquist plots is determined by a disc of radius $|W_P(j\omega)|$. On the other hand, this forbidden neighborhood of the point $[-1, 0j]$ will be given by the robust stability safety margin now. Consequently, some robust performance will be ensured as well, but the further controller design calculations will be much simpler (even without any approximation). The idea of robust relative stability is illustrated in Fig. 7, where the radius $|W_M(j\omega)L_0(j\omega)|$ of the envelope of Nyquist diagrams is multiplied by a margin factor of α. Naturally, for the practical robust stability margin, $\alpha > 1$ is supposed. For $\alpha = 1$, the concept becomes identical with the classic (absolute) robust stability, which can then be considered as a special case.

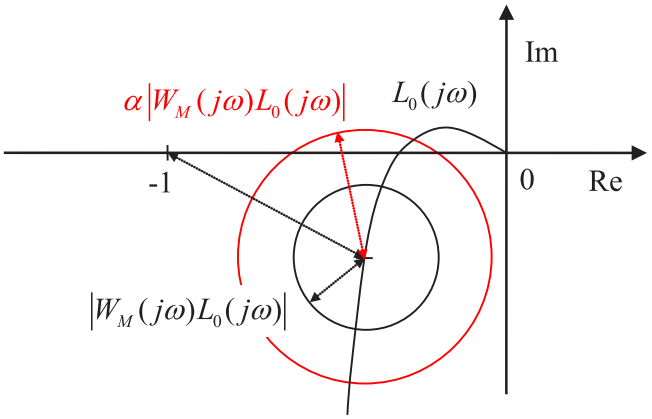

Fig. 7. Graphical interpretation of the robust relative stability condition under multiplicative uncertainty. (For interpretation of the references to colour in this figure legend, the reader is referred to the web version of this article.)

Similarly to the previous Figs. 5 and 6, the drawing in Fig. 7 supposes again a stable open-loop transfer function $L_0(s)$ for simplicity. Then, Fig. 7 depicts that the nominally stable closed-loop system is also robustly relatively stable with a margin factor of α if and only if the critical point $[-1, 0j]$ is excluded from the envelope of Nyquist plots with a radius of $\alpha\,|W_M(j\omega)L_0(j\omega)|$ and the center $L_0(j\omega)$.

Thus, the robust stability condition (12) may be modified to its relativized version as follows: Provided that a nominal closed-loop control system is stable, the corresponding perturbed closed-loop control system is robustly relatively stable with a margin factor of α if and only if:

$$\|W_M(s)T_0(s)\|_\infty < \frac{1}{\alpha}, \tag{30}$$

or alternatively:

$$|T_0(j\omega)| < \frac{1}{\alpha\,|W_M(j\omega)|} \quad \forall\omega. \tag{31}$$

As mentioned above, when compared with the classic robust performance condition (18), the application of the relative stability condition (30) for control design requires less computational effort. On the other hand, the designer has a lower possibility of frequency-based shaping because a frequency-dependent performance weight function $W_P(s)$ is not used anymore, and only $W_M(s)$, as a part of the plant model, is available.

The analogous relative robust stability conditions for additive (4), inverse multiplicative (7), and inverse additive (8) unstructured uncertainty models, respectively, are as follows:

$$\|W_A(s)C(s)S_0(s)\|_\infty < \frac{1}{\alpha}, \tag{32}$$

$$\|W_{IM}(s)G_0(s)S_0(s)\|_\infty < \frac{1}{\alpha}, \tag{33}$$

$$\|W_{IA}(s)S_0(s)\|_\infty < \frac{1}{\alpha}. \tag{34}$$

Now, these robust relative stability conditions (30), (32), (33) or (34) can be utilized in the graphical approach for calculating PID controllers as described in Section 5.1. So, the region of robustly relatively stabilizing parameters can be plotted in the P–I–D space using the trios of P–I–D parameters that meet one of the conditions:

$$\|W_M(s)T_0(s)\|_\infty = \frac{1}{\alpha}, \tag{35}$$

$$\|W_A(s)C(s)S_0(s)\|_\infty = \frac{1}{\alpha}, \tag{36}$$

$$\|W_{IM}(s)G_0(s)S_0(s)\|_\infty = \frac{1}{\alpha}, \tag{37}$$

$$\|W_{IA}(s)S_0(s)\|_\infty = \frac{1}{\alpha}, \tag{38}$$

where the selection of the specific condition depends on the used type of the unstructured uncertainty model, analogously to the previous Section 5.1.

In any case, the P–I–D triplets that fulfill the relevant condition define the surface dividing the P–I–D space into robustly relatively stabilizing and robustly relatively non-stabilizing regions. Thus, the final set of robustly relatively stabilizing controllers can be obtained.

6. Illustrative example 1 — unstructured multiplicative uncertainty

Consider a commonly used first-order plus time delay model of the controlled plant:

$$G_{par}(s, K, T, \Theta) = \frac{K}{Ts+1}e^{-\Theta s}, \tag{39}$$

where all three parameters may vary within the following bounds [15]:

$$K, T, \Theta \in [1, 2]. \tag{40}$$

First, the model with parametric uncertainty (39) has to be replaced by the model with unstructured uncertainty. In fact, the system with parametric uncertainty would not be needed at all here, but it is intentionally used as a preliminary model in this example in order to show the relation with the unstructured uncertainty model, the construction of which resides in the choice of a suitable model type, a nominal system $G_0(s)$, and a weight function, e.g., $W_M(s)$. In [15], the model with unstructured multiplicative uncertainty was created as:

$$\begin{aligned} &G_M(s) = [1 + W_M(s)\Delta_M(s)]\,G_0(s) \\ &\|\Delta_M(s)\|_\infty \le 1 \\ &G_0(s) = \frac{1.5}{1.5s+1} \\ &W_M(s) = \frac{1.\overline{3}s^3 + 2.4481s^2 + 3.2\overline{5}s + 0.\overline{3}}{0.\overline{4}s^3 + 1.\overline{1}s^2 + 1.\overline{6}s + 1} \end{aligned} \tag{41}$$

Note that a time-delay-free nominal model $G_0(s)$ is selected, i.e., the whole time-delay term is considered as the uncertainty, which typically yields the largest uncertainty region, but this choice simplifies the model and thus facilitates the future controller design [13]. Generally, models with unstructured uncertainty that are based on models with parametric uncertainty are more conservative than their parametric counterparts [15].

Fig. 8 [15] presents the comparison of Bode magnitude plots of the weight function $W_M(s)$ and a sampled set of the normalized perturbations $\left(\frac{G_M(s)}{G_0(s)} - 1\right)$ for all variations of parameters with chosen steps for the gain $K = 1:0.1:2$, time constant $T = 1:0.1:2$ as well as time-delay term $\Theta = 1:0.1:2$. Thus, there are $11^3 = 1331$ Bode magnitude curves of the samples of the normalized perturbations (blue curves) and one Bode magnitude curve of the weight $W_M(s)$ (black curve) in Fig. 8 [15]. Then, Fig. 9 [15] is a zoomed version of Fig. 8 [15] and provides a more detailed view. As can be seen, $W_M(s)$ covers the normalized perturbations from above for all frequencies, which means that the inequality (3) is fulfilled.

Suppose that the controlled system with unstructured multiplicative uncertainty (41) is in the classic feedback loop with the

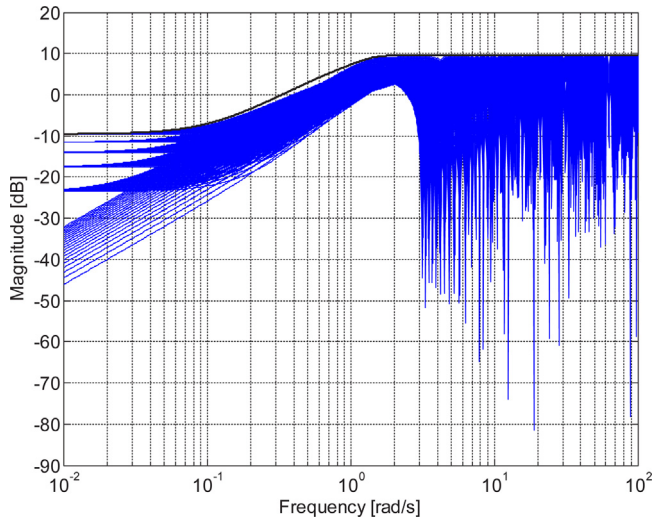

Fig. 8. Bode magnitude plots — the sampled set of normalized perturbations and weight function W_M [15]. (For interpretation of the references to color in this figure legend, the reader is referred to the web version of this article.)

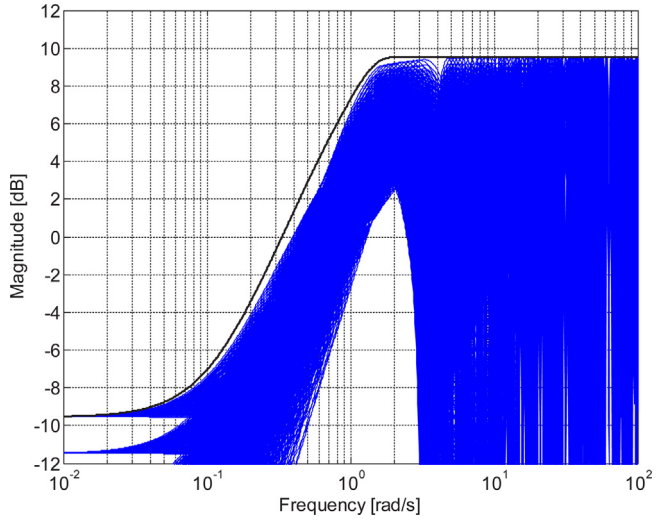

Fig. 9. Zoomed version of Bode magnitude plots from Fig. 8 [15]. (For interpretation of the references to color in this figure legend, the reader is referred to the web version of this article.)

ideal PID controller:

$$C(s) = \frac{k_P s + k_I + k_D s^2}{s}. \tag{42}$$

In accordance with the conditions (12) and (30), the value of $\|W_M(s)T_0(s)\|_\infty$ is critical for decision on robust stability and robust relative stability, and of course, this value depends on the parameters of PID controller (42). For an illustration of this dependence, a 3D plot of the values of $\|W_M(s)T_0(s)\|_\infty$ for various variations of parameters k_P and k_I, with the fixed parameter k_D, is shown in Fig. 10. The parameters k_P and k_I are sampled by $k_P = -5:0.1:5$ and $k_I = -5:0.1:5$, while $k_D = 0.1$.

Obviously, the value $\|W_M(s)T_0(s)\|_\infty = 1$ is the most important from the robust stability border viewpoint (see (26)), and thus the corresponding contour is plotted in Fig. 11. The inequality $\|W_M(s)T_0(s)\|_\infty < 1$ holds true inside the contour. It is obtained by the numerical procedure, in which the parameters k_P and k_I are sampled with step 0.001, and the points that fulfill:

$$|\|W_M(s)T_0(s)\|_\infty - 1| < 0.001 \tag{43}$$

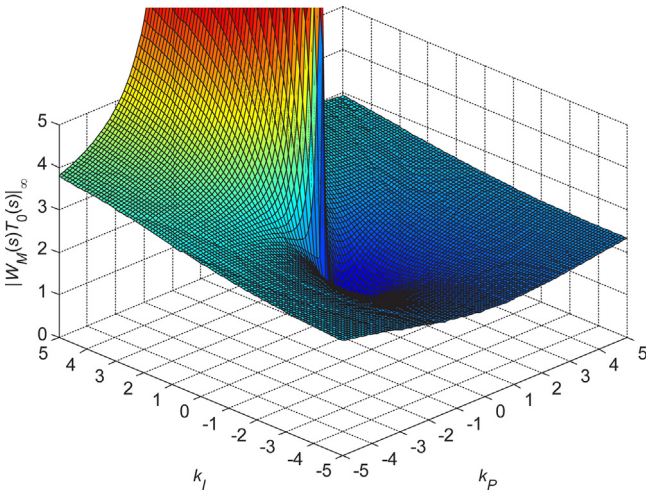

Fig. 10. Values of $\|W_M(s)T_0(s)\|_\infty$ for the fixed $k_D = 0.1$ and a selected range of k_P and k_I.

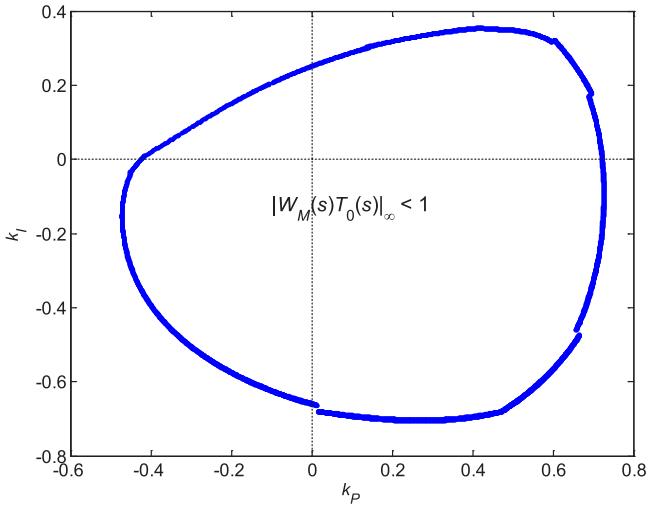

Fig. 11. Contour $\|W_M(s)T_0(s)\|_\infty = 1$ forming the boundary of the internal $\|W_M(s)T_0(s)\|_\infty < 1$ area in a P-I plane for the fixed $k_D = 0.1$.

are included in the plotted curve. In other words, the set of points for which the equality $\|W_M(s)T_0(s)\|_\infty = 1$ is met with the tolerance of one per mille is used for drawing.

The inside of the depicted shape in Fig. 11 could be expected to represent the robust stability region because the condition (12) is satisfied for all relevant internal trios of k_P, k_I, and (fixed) k_D. However, the true robust stability region is also restricted by $k_I = 0$ line, since negative k_I makes the control loop unstable. On the other hand, negative k_P, as well as negative k_D, are theoretically allowed as they can robustly stabilize the control system, but they will not be preferred in practice. All in all, the region of robustly stabilizing PID controllers with $k_D = 0.1$ for the controlled system with unstructured multiplicative uncertainty (41) is shown in Fig. 12. Note that if k_D is fixed at 0, a similar robustly stabilizing region will be obtained for a PI controller as a special case of a PID controller [32].

In order to calculate the final region of robustly stabilizing PID controllers, the same procedure of computing the partial P-I regions (Fig. 12) is repeated for a sampled set of k_D parameters. Fig. 13 shows the region of robustly stabilizing PID controllers for $k_D = -0.25:0.1:0.5$. Note that the values $k_D = -0.25$ and $k_D =$

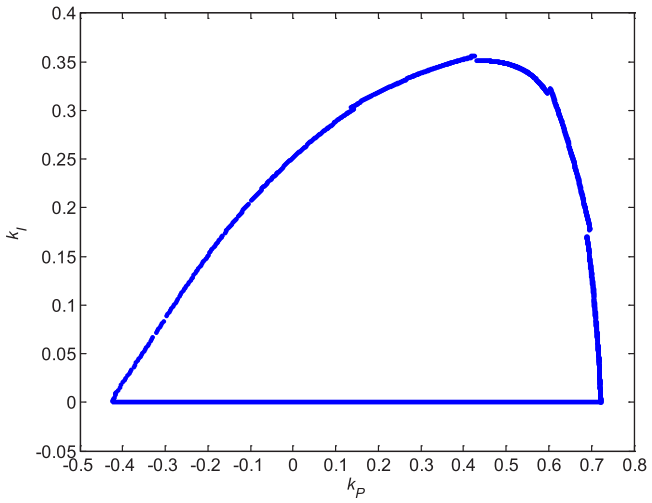

Fig. 12. Robust stability region for the plant (41) and for the fixed $k_D = 0.1$.

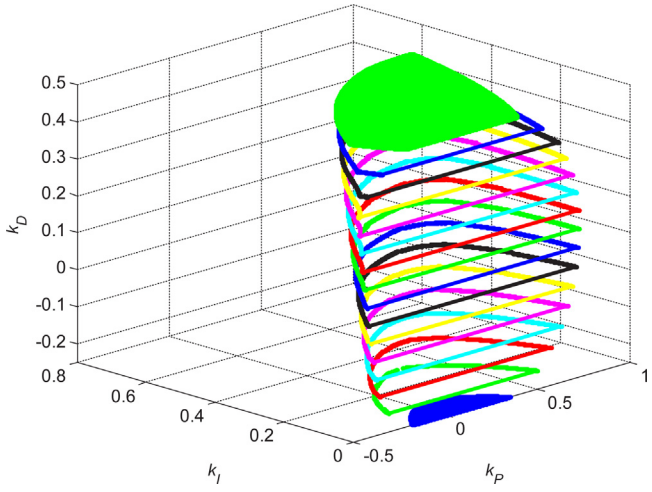

Fig. 13. Region of robustly stabilizing PID controllers for the plant (41).

0.5 represent the minimum and maximum limits (with respect to the assumed sampling) of the robust stability region, respectively, since no variations of parameters k_P, k_I, and k_D for $k_D \lessapprox -0.25$ or $k_D \gtrapprox 0.5$ would fulfill $\|W_M(s)T_0(s)\|_\infty < 1$, i.e., no corresponding controllers would robustly stabilize the model (41). On the other hand, all possible variations of the parameters k_P, k_I, and k_D inside the robust stability region from Fig. 13 guarantee robust stability of the control system with the relevant PID controller and the model with unstructured multiplicative uncertainty (41).

In the next step, the attention will be focused on the calculation of the region of robustly relatively stabilizing PID controllers. The overall computation procedure remains the same as for the previous robustly stabilizing case, but the condition that must be fulfilled by all boundary trios of k_P, k_I, and k_D now changes from (26) to (35), where the margin factor is supposed to be $\alpha = 2$. So, the utilized robust relative stability condition (30) is:

$$\|W_M(s)T_0(s)\|_\infty < \frac{1}{2}, \tag{44}$$

and the boundary trios of P–I–D parameters have to meet the condition (35):

$$\|W_M(s)T_0(s)\|_\infty = \frac{1}{2}. \tag{45}$$

Analogously to the previous robust (absolute) stability case, the practical calculations of individual k_D-sampled contours are based on the numerical approach where the parameters k_P and k_I are sampled with step 0.001, and where the accepted tolerance is one per mille, that is, the following formula is applied:

$$|\|W_M(s)T_0(s)\|_\infty - 0.5| < 0.001. \tag{46}$$

Then, again, the calculations of partial P-I regions are repeated for a sampled set of k_D, now specifically for $k_D = -0.14 : 0.02 : 0.2$, because the values $k_D = -0.14$ and $k_D = 0.2$ represent the minimum and maximum limits of the robust relative stability region, respectively, with respect to the assumed sampling.

Finally, the region of robustly relatively stabilizing PID controllers, for which all possible variations of the parameters k_P, k_I, and k_D inside it fulfill $\|W_M(s)T_0(s)\|_\infty < 0.5$, is plotted in Fig. 14. Thus, Fig. 14 shows the region that guarantees robust relative stability with the margin factor $\alpha = 2$(and consequently a certain degree of robust performance as well) of the control system with the relevant PID controller and the model with unstructured multiplicative uncertainty (41).

The comparison of both robust stability and robust relative stability regions is presented in Fig. 15. Naturally, the region of robustly relatively stabilizing PID controllers (depicted by red color) comprises the subset of the region of robustly stabilizing PID controllers (depicted by blue color). Obviously, similar greater or smaller subsets could be obtained for smaller or greater values of the margin factor $\alpha > 1$, respectively.

7. Illustrative example 2 – unstructured additive uncertainty

Consider a third-order plant with integrating behavior, inspired by Examples 6.4, 6.5, and 9.5 from [56]:

$$G_{par}(s, a_1, a_2) = \frac{1}{s\left(s^2 + a_2 s + a_1\right)} = \frac{1}{s^3 + a_2 s^2 + a_1 s} \tag{47}$$

with the parameters lying within the bounds:

$$\begin{matrix} a_1 \in [3, 5] \\ a_2 \in [1, 3] \end{matrix}. \tag{48}$$

Similarly to the previous example, the preliminary model with uncertain parameters (47) will be replaced by the model with unstructured uncertainty. More specifically, the model with unstructured additive uncertainty that was constructed in [57] will be utilized:

$$\begin{matrix} G_A(s) = G_0(s) + W_A(s)\Delta_A(s) \\ \|\Delta_A(s)\|_\infty \le 1 \\ G_0(s) = \dfrac{1}{s^3 + 2s^2 + 4s} \\ W_A(s) = \dfrac{0.09\,(7s+1)}{s\,(0.5s+1)^4} \end{matrix}. \tag{49}$$

The comparison of Bode magnitude plots of the weight function $W_A(s)$ and a sampled set of the normalized perturbations $(G_A(s) - G_0(s))$ for all variations of parameters with chosen steps $a_1 = 3 : 0.1 : 5$ and $a_2 = 1 : 0.1 : 3$ is shown in Fig. 16 [57]. Consequently, Fig. 16 contains $21^2 = 441$ Bode magnitude curves of the samples of the normalized perturbations (blue curves) and one Bode magnitude curve of the weight $W_A(s)$ (black curve). In compliance with the inequality (5), weight $W_A(s)$ is selected in order to cover the normalized perturbations from above for all frequencies.

Consider that the feedback control system consists of the controlled plant described by the model with unstructured additive

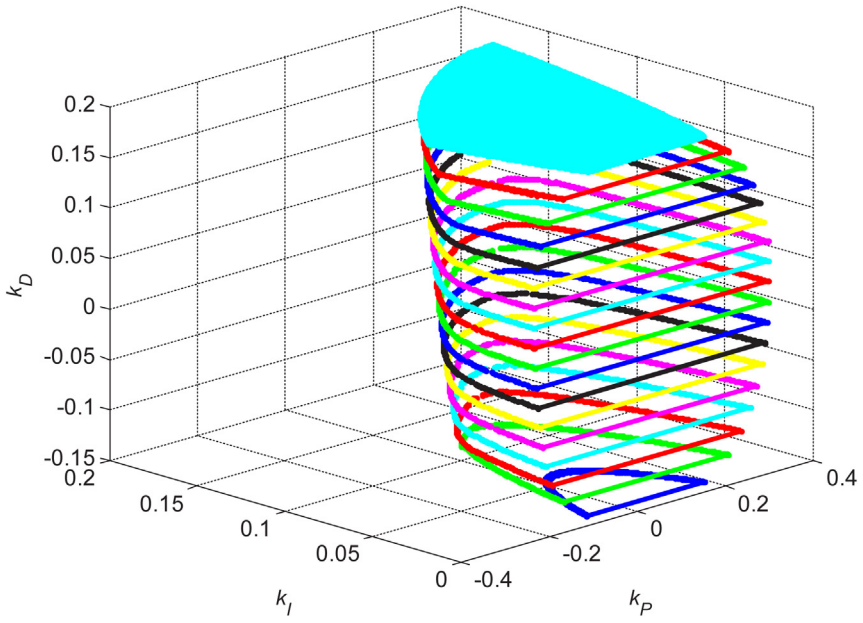

Fig. 14. Region of robustly relatively stabilizing PID controllers for the plant (41) and for $\alpha = 2$.

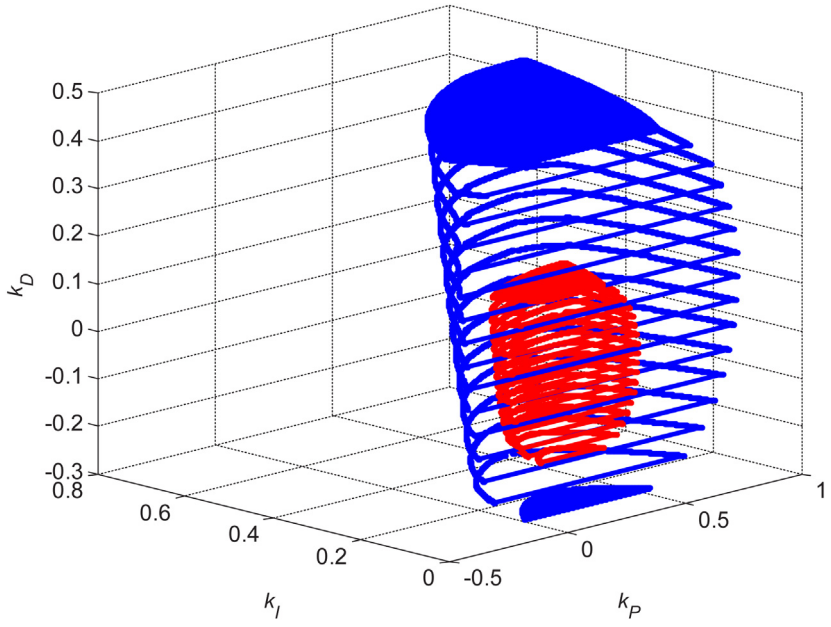

Fig. 15. Regions of robustly stabilizing (blue) and robustly relatively stabilizing (red) PID controllers for the plant (41).. (For interpretation of the references to color in this figure legend, the reader is referred to the web version of this article.)

uncertainty (49) and the ideal PID controller (42), similarly as in the previous Example 1.

Under unstructured additive uncertainty, the controller–parameter-dependent value of $\|W_A(s)C(s)S_0(s)\|_\infty$ is essential for a decision on robust stability (see condition (15)) or robust relative stability (see condition (32)). For example, the contour $\|W_A(s)C(s)S_0(s)\|_\infty = 1$ is plotted in Fig. 17 for $k_D = -0.1$, and the inequality $\|W_A(s)C(s)S_0(s)\|_\infty < 1$ holds true inside this shape. The contour is achieved by the following numerical way: The parameters k_P and k_I are sampled with step 0.005, and the contour consists of the points that comply with:

$$|\|W_A(s)C(s)S_0(s)\|_\infty - 1| < 0.001. \tag{50}$$

Thus, analogously to Fig. 11, the shape in Fig. 17 is practically composed of the points for which the equality $\|W_A(s)C(s)S_0(s)\|_\infty = 1$ is fulfilled with the tolerance of one per mille.

Despite the fact that all relevant internal trios of k_P, k_I, and (fixed) k_D parameters from Fig. 17 satisfy the condition (15), the depicted shape is actually not the genuine robust stability region, because negative k_I would make the control system unstable, and consequently, the robust stability region is bounded by $k_I = 0$ line from below. Nevertheless, analogously to the previous Example 1, negative k_P and/or negative k_D are theoretically permissible, since they may still lead to a robustly stable control loop — see Fig. 18, where the true region of robustly stabilizing PID controllers, even for negative $k_D = -0.1$ and potentially negative k_P, is drawn. In

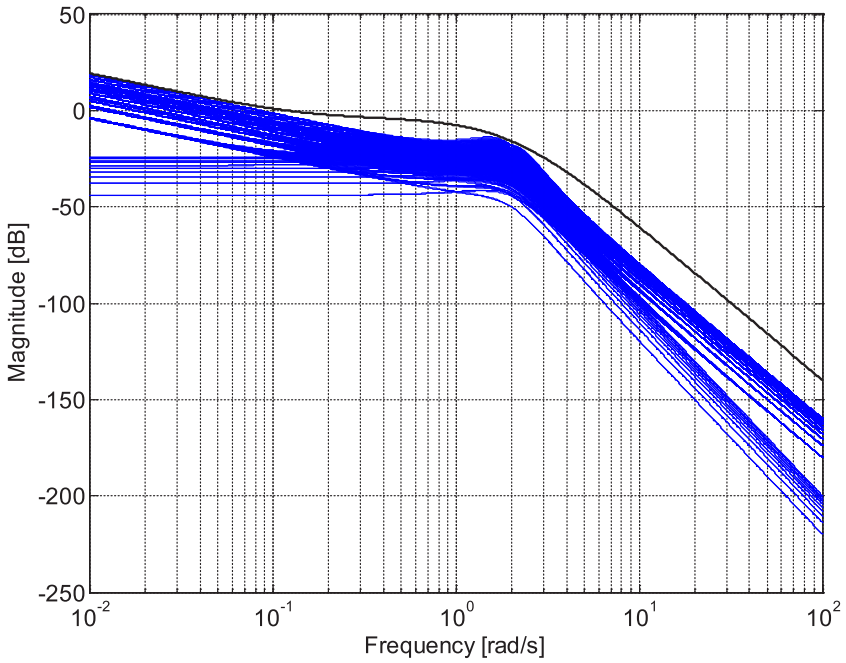

Fig. 16. Bode magnitude plots — the sampled set of normalized perturbations and weight function W_A [57]. (For interpretation of the references to color in this figure legend, the reader is referred to the web version of this article.)

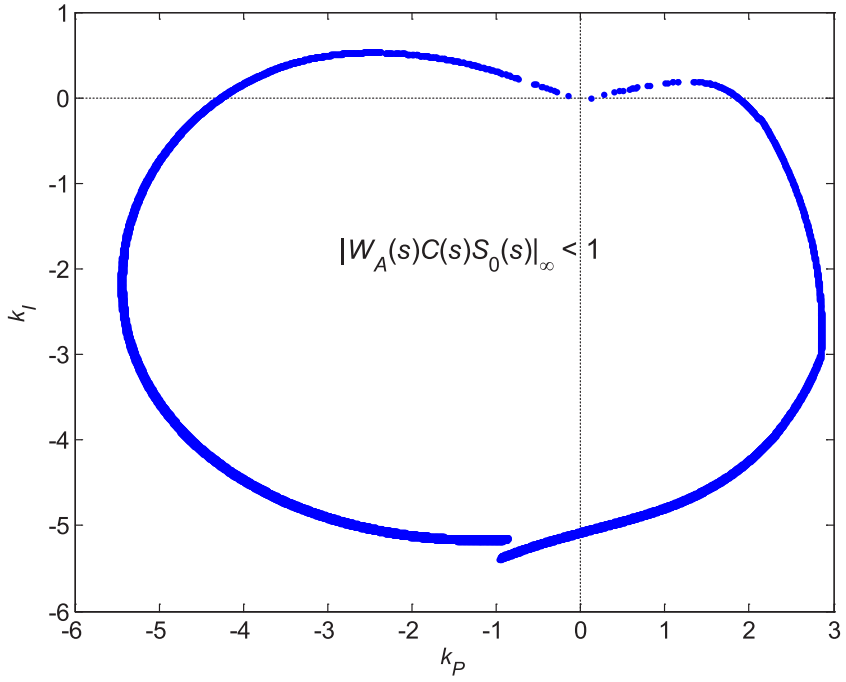

Fig. 17. Contour $\|W_A(s)C(s)S_0(s)\|_\infty = 1$ forming the boundary of the internal $\|W_A(s)C(s)S_0(s)\|_\infty < 1$ area for the fixed $k_D = -0.1$.

Fig. 18, the parameters k_P and k_I are sampled with step 0.001, and the tolerance (50) is used again.

As can be seen in Fig. 18, the large part of the robust stability region comes under negative values of k_P and also k_D in this example. However, negative controller parameters would not be preferred in practice, so they will be omitted in the following figures for better lucidity, i.e., the presented final robust stability and robust relative stability regions (Figs. 20 and 21) will be restricted only to the nonnegative controller parameters. But before that, an example of the restricted version of the robust stability region for the fixed k_D (from Fig. 18) is plotted in Fig. 19, where only nonnegative values of k_P are considered (nevertheless, the whole region is still obtained for negative $k_D = -0.1$).

The same process of calculating the partial P-I regions (as in Fig. 19) is repeated for a sampled set of k_D parameters, but only for nonnegative values of k_D due to practical reasons mentioned above (more specifically, $k_D = 0:0.2:4$ in this case). It leads to the final restricted region of robustly stabilizing PID controllers for the model with unstructured additive uncertainty (49), as shown in Fig. 20. Obviously, all possible controller parameter variations inside this region guarantee robust stability of the control loop with the relevant PID controller (with nonnegative

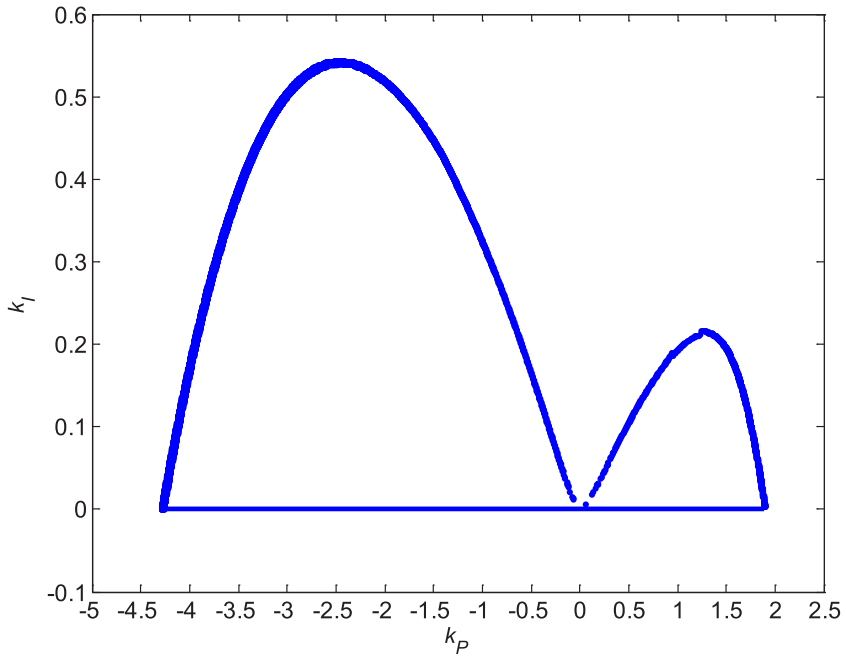

Fig. 18. Robust stability region for the plant (49) and for the fixed $k_D = -0.1$.

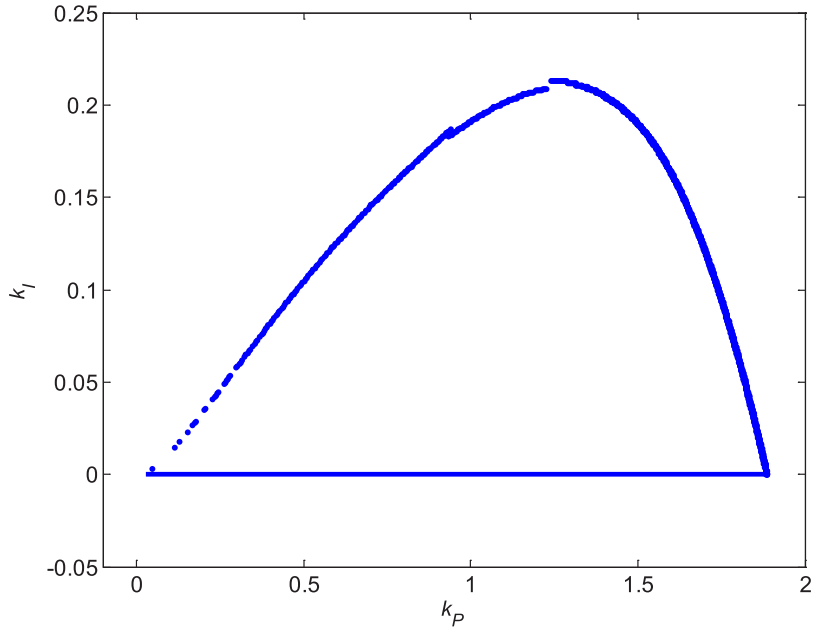

Fig. 19. Robust stability region for the plant (49) and for the fixed $k_D = -0.1$ (restricted to the nonnegative values of k_P).

parameters) and the plant with unstructured additive uncertainty (49).

In the final steps, two various regions of robustly relatively stabilizing PID controllers (with nonnegative parameters) will be calculated. The margin factors will be set at $\alpha = 1.5$ and $\alpha = 2$. Again, the general procedure is analogous to the previous cases, but now the condition (36) is utilized for obtaining the boundary trios of k_P, k_I, and k_D. Thus, for $\alpha = 1.5$ and $\alpha = 2$, the robust relative stability condition (32) takes the form, respectively:

$$\|W_A(s)C(s)S_0(s)\|_\infty < \frac{1}{1.5} = \frac{2}{3}, \tag{51}$$

$$\|W_A(s)C(s)S_0(s)\|_\infty < \frac{1}{2}, \tag{52}$$

and so the boundary trios of controller parameters have to satisfy the condition (36), respectively:

$$\|W_A(s)C(s)S_0(s)\|_\infty = \frac{2}{3}, \tag{53}$$

$$\|W_A(s)C(s)S_0(s)\|_\infty = \frac{1}{2}. \tag{54}$$

For the case $\alpha = 1.5$, the individual k_D-sampled contours ($k_D = 0:0.1:2.4$) are practically obtained by means of the numerical calculations where the parameters k_P and k_I are sampled with step 0.001, and where the accepted tolerance is again one per mille, i.e., the following formula is used:

$$\left|\|W_A(s)C(s)S_0(s)\|_\infty - 0.6\overline{6}\right| < 0.001. \tag{55}$$

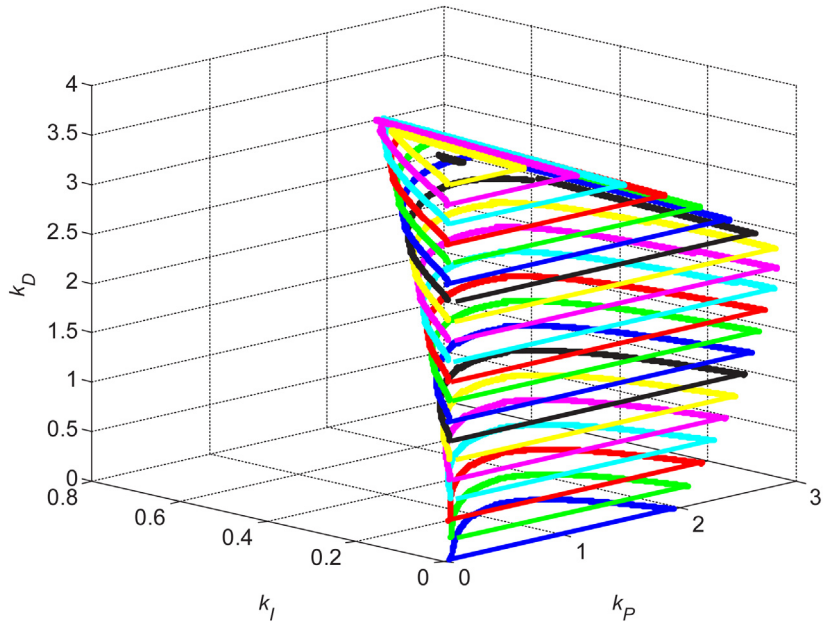

Fig. 20. Region of robustly stabilizing PID controllers for the plant (49) (restricted to the nonnegative controller parameters).

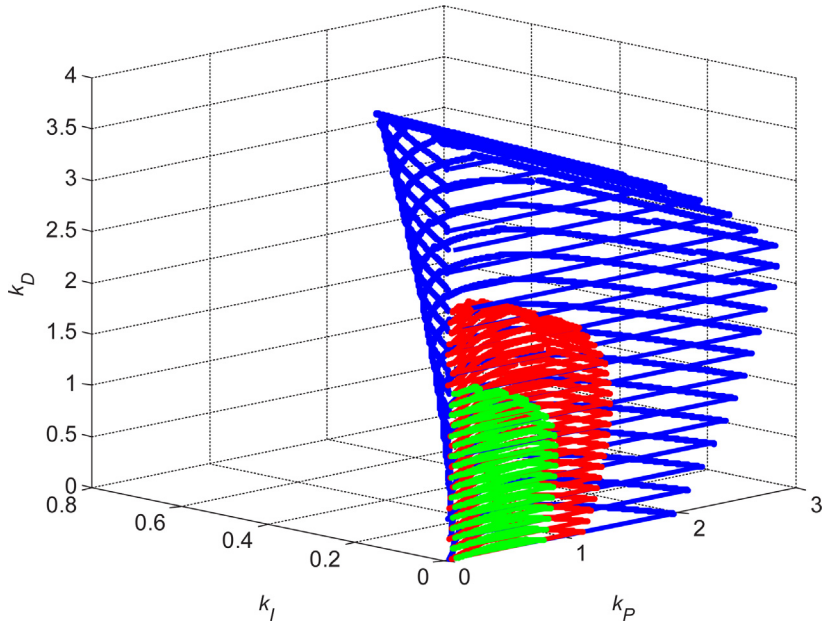

Fig. 21. Regions of robustly stabilizing (blue), robustly relatively stabilizing for $\alpha = 1.5$ (red), and robustly relatively stabilizing for $\alpha = 2$ (green) PID controllers for the plant (49)(restricted to the nonnegative controller parameters).. (For interpretation of the references to color in this figure legend, the reader is referred to the web version of this article.)

Similarly, for the case $\alpha = 2$, the set of P-I contours for $k_D = 0:0.1:1.6$ are computed on the basis of the inequality:

$$|\|W_A(s)C(s)S_0(s)\|_\infty - 0.5| < 0.001. \tag{56}$$

The final Fig. 21 shows the region of robust stability (from Fig. 20, now depicted by blue color) together with both regions of robust relative stability for margin factors $\alpha = 1.5$ (depicted by red color) and $\alpha = 2$ (depicted by green color). With respect to the previous considerations, they are restricted only to the nonnegative controller parameters. Obviously, the robust relative stability region for $\alpha = 2$ (green) is the subset of the robust relative stability region for $\alpha = 1.5$ (red), which is the subset of the robust stability region (blue). Anyway, all possible variations of the nonnegative parameters k_P, k_I, and k_D inside the obtained regions guarantee robust stability or robust relative stability (with some prescribed margin factor and, consequently, with a certain degree of robust performance as well) of the control loop with the relevant PID controller and the plant model with unstructured additive uncertainty (49).

8. Control of airflow speed in a hot-air tunnel

In order to demonstrate the practical applicability of the method to real-life control problems, a robustly relatively stabilizing controller will be designed for the laboratory model of a

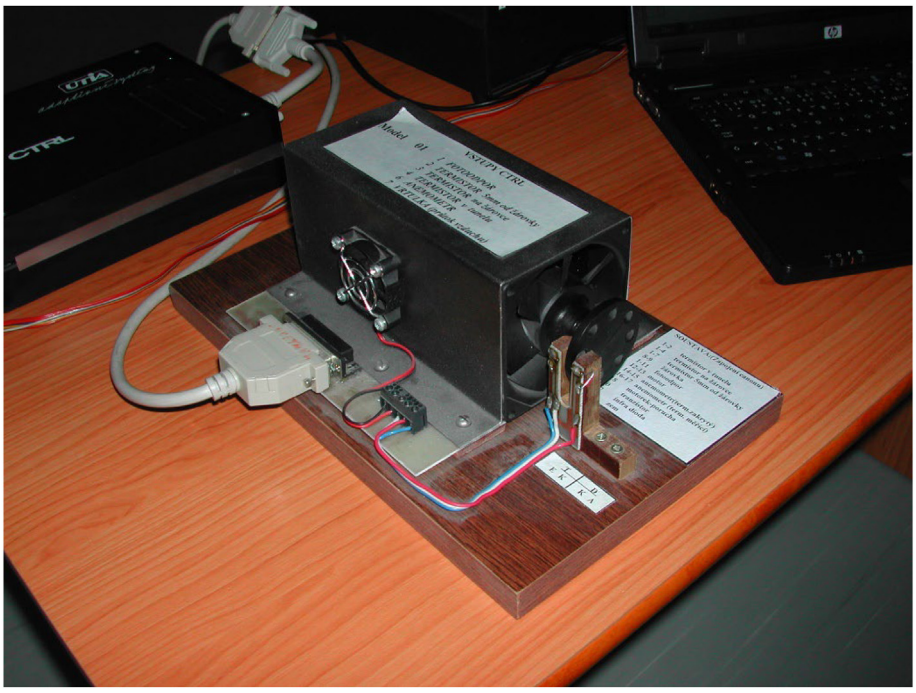

Fig. 22. Laboratory model of the hot-air tunnel.

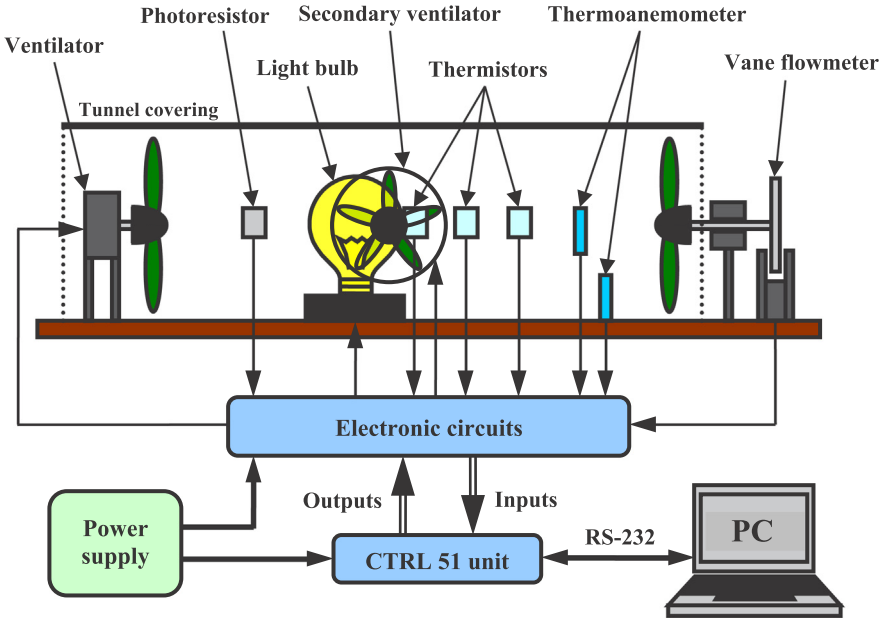

Fig. 23. Diagram of the hot-air tunnel and the whole control system [59–62].

hot-air tunnel, which was constructed in VSB — Technical University of Ostrava [58]. The model consists of the bulb, primary ventilator, secondary ventilator, and several sensors covered by the tunnel. The bulb serves as the source of heat and light energy, and it is powered by a controllable source of voltage. Then, the purpose of controllable ventilators is to ensure the airflow inside the tunnel. Generally, the tunnel is a MIMO system, but the presented control experiment will be performed on a selected SISO loop. The real appearance of the laboratory hot-air apparatus is shown in Fig. 22.

All actuators and sensors are connected via the electronic circuits (adjusting signals to the suitable voltage levels) to the control unit, more specifically CTRL 51 unit, which was created in the Institute of Information Theory and Automation, Academy of Sciences of the Czech Republic [63]. Then, this control unit is connected to the Personal Computer (PC) through the serial link RS-232. More information about the use of the serial link in the Matlab environment, including user routines, program synchronization mechanism, and several tests, can be found in [64]. The scheme of the hot-air tunnel and its connection with the whole control system is shown in Fig. 23 [59–62]. Note that due to better visibility, the secondary ventilator is displayed on the opposite side than it is placed in the real plant.

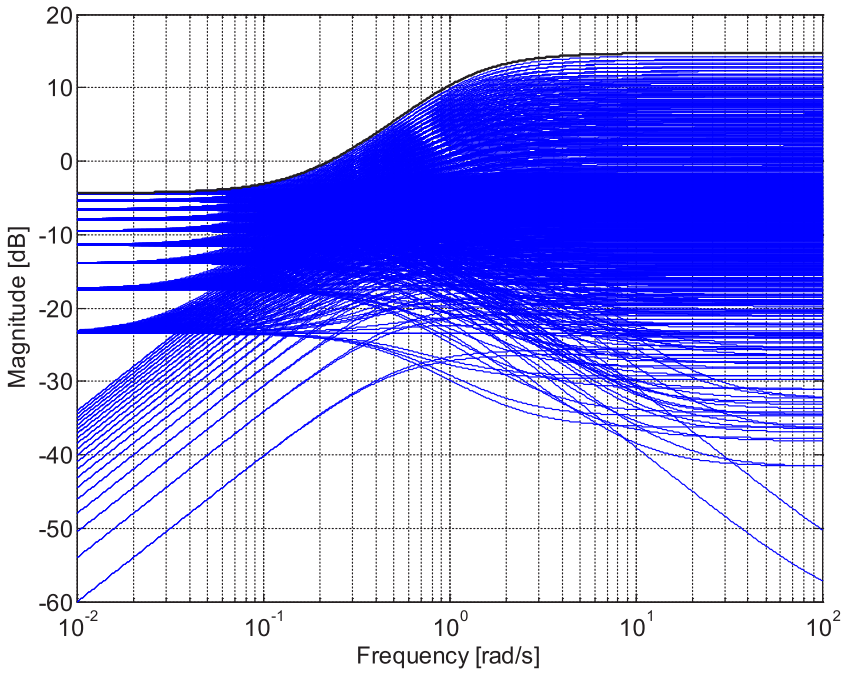

Fig. 24. Bode magnitude plots — the sampled set of normalized perturbations and weight function W_M (60) .. (For interpretation of the references to color in this figure legend, the reader is referred to the web version of this article.)

The considered control loop consists of (primary) ventilator voltage as the control signal (denoted by the $u2$ symbol in accordance with [58,59]) and the airflow speed at the end of the tunnel interpreted by the voltage on the vane flowmeter as the output (controlled) signal (symbolized by $y7$). Two remaining actuating (control) signals, namely, bulb voltage ($u1$) and voltage of the secondary ventilator ($u3$), were set to a constant 0 V. The used symbols correspond with the real connection of input and output channels of CTRL 51 unit. In case of interest, the complete list of all channels, including their meaning, can be found in the works [58,59].

In [59–61], the mathematical model with parametric uncertainty was obtained by means of performing identification experiments at various operational points. More specifically, the controlled plant was identified as the second-order system with a double time constant:

$$G_{par}(s,K,T)=\frac{K}{(Ts+1)^2}, \tag{57}$$

where

$$\begin{matrix} K\in[0.3,\,1.2] \\ T\in[1,\,3] \end{matrix}. \tag{58}$$

The gain is dimensionless [-] and the time constant is given in seconds [s].

With regard to the proposed method, a model with unstructured uncertainty is required. More specifically, the most common model with unstructured multiplicative uncertainty will be constructed in this case, analogously to Section 6 and procedures presented in [15].

The nominal model $G_0(s)$ is selected easily by taking the average values of (58):

$$G_0(s)=\frac{0.75}{(2s+1)^2}. \tag{59}$$

Then, the selection of a suitable weight function $W_M(s)$ is based on a natural technique from [15]. It grounds in the idea that the worst-case uncertainty is obtained for the controlled plant (57) with the greatest possible gain $K=1.2$ and the shortest possible double time constant $T=1$. Such a combination directly leads to the "uppermost" normalized perturbation Bode magnitude characteristics. Thus, the selected weight function $W_M(s)$ has the form:

$$W_M(s)=\frac{27s^2+22s+3}{5s^2+10s+5}. \tag{60}$$

The comparison of Bode magnitude diagram of (60) and Bode magnitude diagrams of a sampled set of the normalized perturbations $\left(\frac{G_M(s)}{G_0(s)}-1\right)$ for all variations of parameters $K=0.3:0.05:1.2$ and $T=1:0.05:3$ is shown in Fig. 24. Analogously to the previous similar figures, $19\cdot 41=779$ blue curves correspond to the samples of the normalized perturbations and one black curve represents the weight function (60). Moreover, Fig. 25 is a zoomed version of Fig. 24 and it clearly shows that Bode magnitude plot of (60) covers Bode magnitude plots of normalized perturbations in the tightest possible way. In other words, the inequality (3) is fulfilled marginally in this case.

All in all, the final model with unstructured multiplicative uncertainty is considered as:

$$\begin{matrix} G_M(s)=[1+W_M(s)\Delta_M(s)]\,G_0(s) \\ \|\Delta_M(s)\|_\infty\le 1 \\ G_0(s)=\dfrac{0.75}{(2s+1)^2} \\ W_M(s)=\dfrac{27s^2+22s+3}{5s^2+10s+5} \end{matrix}. \tag{61}$$

Suppose that the airflow speed in the hot-air tunnel, modeled by (61), is controlled by PID controller (42). For the sake of practical implementation, the emulation of ideal continuous-time PID control law by means of the discrete-time algorithm was performed using the backward rectangular rule, sampling period 0.1 s, and a suitable filter for the derivative term.

Analogously to Illustrative Example 1, the $\|W_M(s)T_0(s)\|_\infty<1$ area could be plotted for a fixed k_D. Nevertheless, in this case,

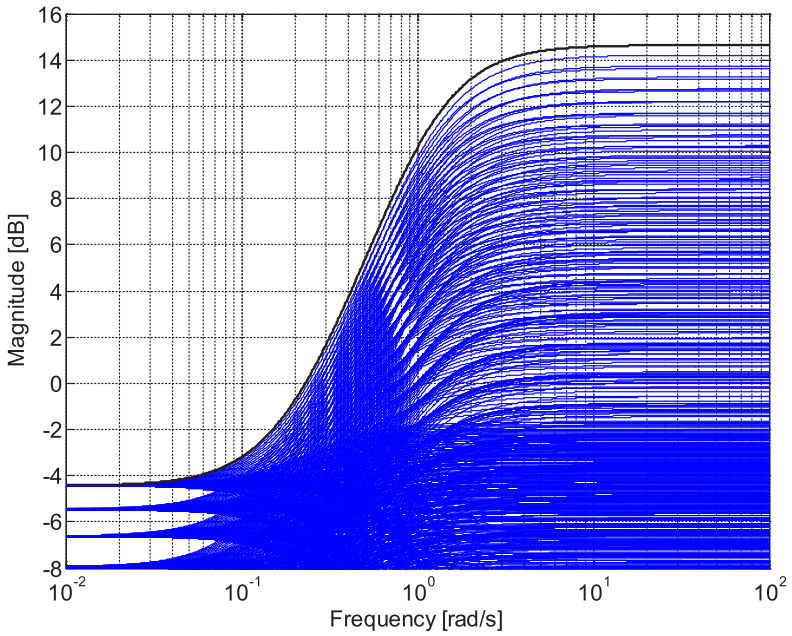

Fig. 25. Zoomed version of Bode magnitude plots from Fig. 24. (For interpretation of the references to color in this figure legend, the reader is referred to the web version of this article.)

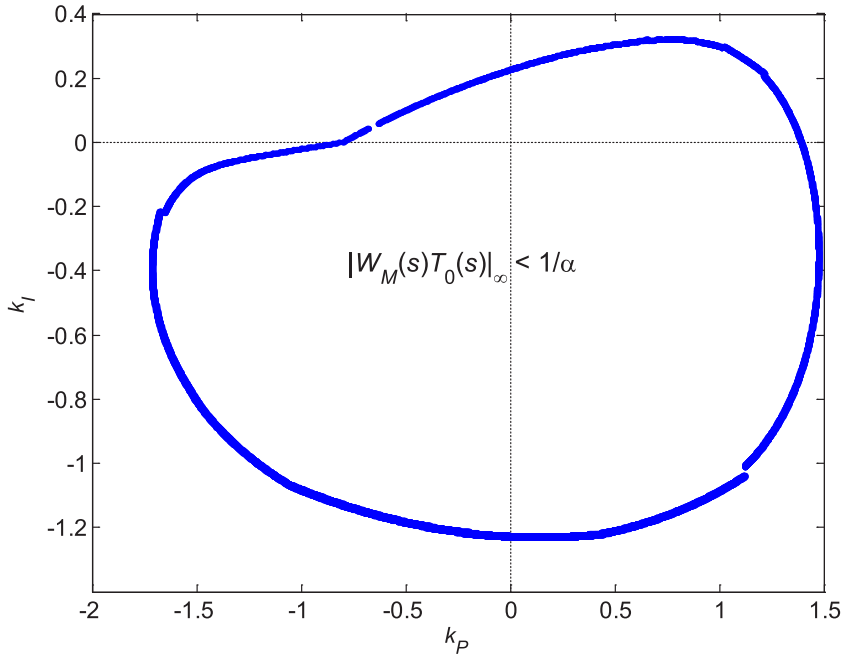

Fig. 26. Contour $\|W_M(s)T_0(s)\|_\infty = 1/\alpha$ forming the boundary of the internal $\|W_M(s)T_0(s)\|_\infty < 1/\alpha$ area in a P-I plane for the fixed $k_D = 0.1$ and $\alpha = 1.1$.

robust relative stability scenario $\|W_M(s)T_0(s)\|_\infty < 1/\alpha$ is considered directly, with the specific value of margin factor $\alpha = 1.1$. In practical calculations, the parameters k_P and k_I are sampled with step 0.001, and the tolerance of one per mille is supposed. The corresponding curve forming the boundary of $\|W_M(s)T_0(s)\|_\infty < 0.\overline{90}$ area in a P-I plane for $k_D = 0.1$ is plotted in Fig. 26.

Following the discussion in the previous two academic examples (Illustrative Examples 1 and 2), the regions of robustly relatively stabilizing PID controllers will be restricted to the nonnegative controller parameters only. Such limited robust relative stability region in a P-I plane for the fixed $k_D = 0.1$ is shown in Fig. 27.

The definitive region of robustly relatively stabilizing PID controllers, restricted to the nonnegative values of the controller parameters, is depicted in Fig. 28. As before, it is obtained by means of repeating the previous procedure (from Fig. 27) for a sampled set of nonnegative parameters k_D (with step 0.1 in this case). Evidently, all possible variations of nonnegative-parameter PID controllers from the inside of the region shown in Fig. 28 ensure robust relative stabilization of the airflow speed in the hot-air

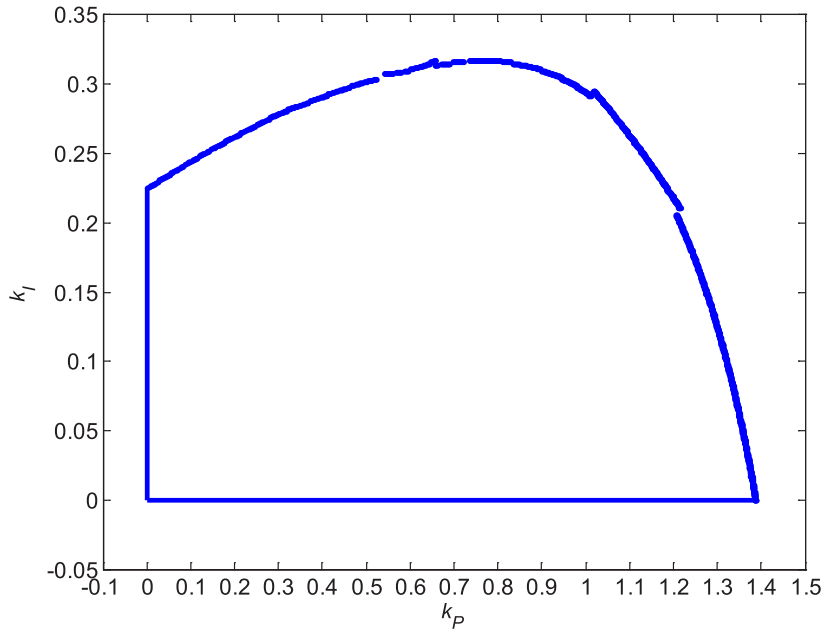

Fig. 27. Robust relative stability region for the model (61) of airflow speed in the hot-air tunnel and for the fixed $k_D = 0.1$ (restricted to the nonnegative values of k_P).

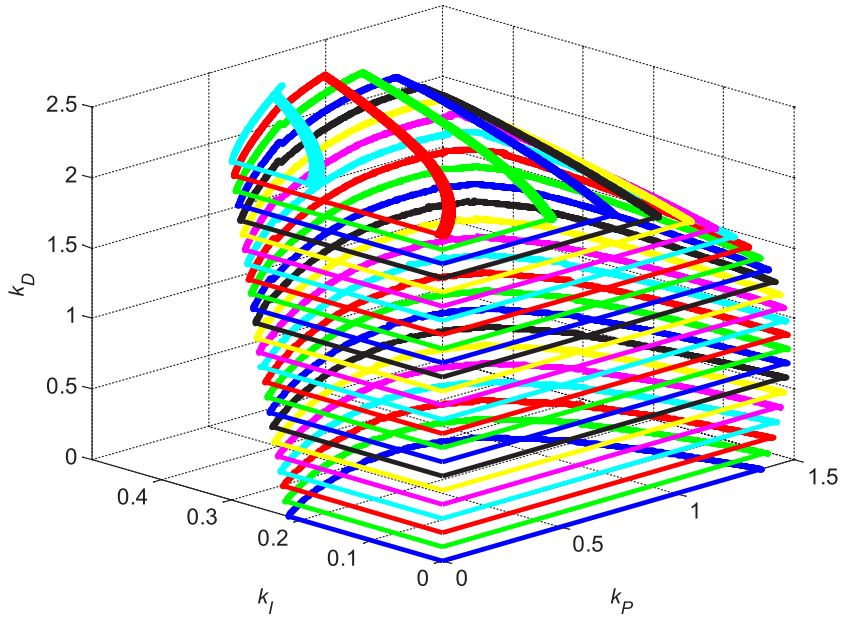

Fig. 28. Region of robustly relatively stabilizing PID controllers for the model (61) of airflow speed in the hot-air tunnel (restricted to the nonnegative controller parameters).

tunnel, modeled as the system with unstructured multiplicative uncertainty (61).

Two specific controllers, $C_1(s)$ and $C_2(s)$, were selected from the robust relative stability region (Fig. 28) and applied to control the speed of airflow in the hot-air apparatus by means of their discrete-time emulation as described above. The parameters of these controllers are as follows:

$$\begin{aligned} &C_1(s): k_P = 1, k_I = 0.27, k_D = 0 \\ &C_2(s): k_P = 1, k_I = 0.32, k_D = 0.3 \end{aligned}. \tag{62}$$

As can be seen, the proportional and integral terms were chosen at the higher levels of possible values determined by the robust relative stability region (Fig. 28), while the derivative terms are from the lower areas. Actually, $C_1(s)$ is a special case since it represents the PI controller. The performance of both PI controller $C_1(s)$ and PID controller $C_2(s)$ is shown in Fig. 29. It contains one black curve defining the reference signal, two blue curves demonstrating the behavior of controller $C_1(s)$, and two red curves related to controller $C_2(s)$. For both controllers, there is an output (controlled) signal approaching the reference, and a control (actuating) signal.

The responses from Fig. 29 indicate that controller $C_2(s)$ has a shorter settling time but, on the other hand, also a more aggressive and jittering control signal when compared to $C_1(s)$. Anyway, both controllers exhibit generally acceptable behavior. Nevertheless, the final choice of some specific controller from the

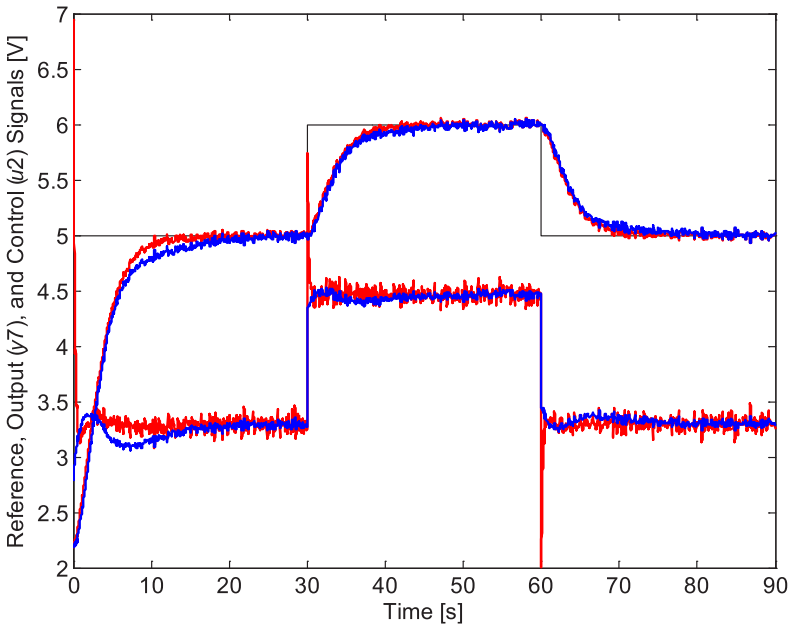

Fig. 29. Control of airflow speed in the hot-air tunnel using controllers $C_1(s)$ (blue curves) and $C_2(s)$ (red curves).. (For interpretation of the references to color in this figure legend, the reader is referred to the web version of this article.)

robust relative stability region (Fig. 28) would depend on further preferences.

9. Conclusions

The paper was focused on the computation of regions of robustly relatively stabilizing PID controllers with some given robust stability margin α (typically $\alpha > 1$) for LTI systems affected by unstructured uncertainty. The procedure is based on plotting the envelope corresponding to the trios of P–I–D parameters that marginally comply with a robust relative stability condition formulated via the H_∞ norm. Moreover, the presented method may also result in the region of robustly (absolutely) stabilizing PID controllers as a special case for $\alpha = 1$. The unstructured uncertainty presented in the plant model can be of any common type. The key contribution of this work consists in the extension of the method for PID controllers and its generalization for the concept of robust relative stability. The applicability of the theoretical results is shown not only in the illustrative examples but also practically verified by means of the real control experiments on the laboratory model of the hot-air tunnel.

Declaration of competing interest

The authors declare that they have no known competing financial interests or personal relationships that could have appeared to influence the work reported in this paper.

Acknowledgments

This work was supported by the Czech Science Foundation (GACR) under Grant No. 21-45465L.

References

[1] Researchgatenet. What is the percentage of the pid algorithm applications in industry? 2021, [online], Available from URL: <https://www.researchgate.net/post/What_is_the_percentage_of_the_PID_algorithm_applications_in_industry>. [Accessed 09 September 2021].

[2] O'Dwyer A. Handbook of PI and PID controller tuning rules. 3rd ed.. London, UK: Imperial College Press; 2009.

[3] Desborough L, Miller R. Increasing customer value of industrial control performance monitoring-honeywell's experience. In: Chemical process control-VI, assessment and new directions for research – Proceedings of the sixth international conference on chemical process control. AIChE symposium series, vol. 98, (no. 326):American Institute of Chemical Engineers; 2002, p. 169–89.

[4] Samad T. A survey on industry impact and challenges thereof [Technical activities]. IEEE Control Syst Mag 2017;37(1):17–8. http://dx.doi.org/10.1109/MCS.2016.2621438.

[5] Ge M, Chiu M-S, Wang Q-G. Robust PID controller design via LMI approach. J Process Control 2002;12(1):3–13. http://dx.doi.org/10.1016/S0959-1524(00)00057-3.

[6] Vilanova R, Alfaro VM, Arrieta O. Robustness in PID control. In: Vilanova R, Visioli A, editors. PID control in the third millennium, advances in industrial control. London: Springer; 2012, http://dx.doi.org/10.1007/978-1-4471-2425-2_4.

[7] Vilanova R, Arrieta O, Ponsa P. Robust PI/PID controllers for load disturbance based on direct synthesis. ISA Trans 2018;81:177–96.

[8] Bhattacharyya SP. Robust control under parametric uncertainty: An overview and recent results. Annu Rev Control 2017;44:45–77.

[9] Bhattacharyya SP, Datta A, Keel LH. Linear control theory: Structure, robustness, and optimization. Group, Boca Raton, Florida, USA: CRC Press, Taylor & Francis; 2009.

[10] Barmish BR. New tools for robustness of linear systems. New York, USA: Macmillan; 1994.

[11] Ackermann J, Bartlett A, Kaesbauer D, Sienel W, Steinhauser R. Robust control – Systems with uncertain physical parameters. London, UK: Springer-Verlag; 1993.

[12] Doyle JC, Francis B, Tannenbaum A. Feedback control theory. New York, USA: Macmillan; 1992.

[13] Skogestad S, Postlethwaite I. Multivariable feedback control: Analysis and design. Chichester, UK: John Wiley and Sons; 2005.

[14] Kučera V. Robustní regulátory (robust controllers). rvtAuto 2001;7(6):43–5, (In Czech).

[15] Matušů R, Şenol B, Yeroğlu C. Linear systems with unstructured multiplicative uncertainty: Modeling and robust stability analysis. PLoS One 2017;12(7).

[16] Matušů R, Prokop R, Pekař L. Parametric and unstructured approach to uncertainty modelling and robust stability analysis. Int J Math Models Methods Appl Sci 2011;5(6):1011–8.

[17] Doyle JC. Synthesis of robust controllers and filters. In: Proceedings of the 22nd IEEE conference on decision and control. San Antonio, Texas, USA; 1983, p. 109–14.

[18] Zhou K, Doyle JC, Glover K. Robust and optimal control. Upper Saddle River, New Jersey, USA: Prentice Hall; 1996.

[19] Yang J, Zhu Y, Yin W, Hu C, Yang K, Mu H. LFT structured uncertainty modeling and robust loop-shaping controller optimization for an ultraprecision positioning stage. IEEE Trans Ind Electron 2014;61(12):7013–25.

[20] Pfifer H, Hecker S. Generation of optimal linear parametric models for LFT-based robust stability analysis and control design. IEEE Trans Control Syst Technol 2011;19(1):118–31.
[21] Söylemez MT, Bayhan N. Calculation of all H_∞ robust stabilizing gains for SISO LTI systems. IFAC Proc Vol 2008;41(2):3982–7. http://dx.doi.org/10.3182/20080706-5-KR-1001.00670.
[22] Matušů R, Şenol B, Pekař L. Robust stability of fractional-order linear time-invariant systems: Parametric versus unstructured uncertainty models. Complexity 2018;2018. http://dx.doi.org/10.1155/2018/8073481.
[23] Sarjaš A, Svečko R, Chowdhury A. Strong stabilization servo controller with optimization of performance criteria. ISA Trans 2011;50(3):419–31. http://dx.doi.org/10.1016/j.isatra.2011.03.005.
[24] Lao Y, Scruggs JT. Robust control of wave energy converters using unstructured uncertainty. In: Proceeding of the 2020 American control conference. Denver, CO, USA; 2020, p. 4237–44. http://dx.doi.org/10.23919/ACC45564.2020.9148045.
[25] Ramos ETG, Acioli G, Barros PR, Neto JSR. H_∞ Robust control using LMI and unstructured uncertainty applied to a temperature process. In: Proceedings of the 2020 7th international conference on control, decision and information technologies. Prague, Czech Republic; 2020, p. 1087–92. http://dx.doi.org/10.1109/CoDIT49905.2020.9263954.
[26] Zhai G, Murao S, Koyama N, Yoshida M. Low order H_∞ controller design: An LMI approach. In: Proceedings of the 2003 European control conference. 2003, p. 3070–5. http://dx.doi.org/10.23919/ECC.2003.7086510.
[27] Ankelhed D. On design of low order H-infinity controllers [Doctoral dissertation], Linköping, Sweden: Linköping University; 2011.
[28] Mitchell T, Overton ML. Fixed low-order controller design and H_∞ optimization for large-scale dynamical systems. IFAC-PapersOnLine 2015;48(14):25–30. http://dx.doi.org/10.1016/j.ifacol.2015.09.428.
[29] Ho M-T. Synthesis of H_∞ PID controllers: A parametric approach. Automatica 2003;39(6):1069–75.
[30] Tsakalis KS, Dash S. Approximate H_∞ loop shaping in PID parameter adaptation. Internat J Adapt Control Signal Process 2013;27(1–2):136–52. http://dx.doi.org/10.1002/acs.2350.
[31] Han S, Keel LH, Bhattacharyya SP. Pid controller design with an H_∞ criterion. IFAC-PapersOnLine 2018;51(4):400–5. http://dx.doi.org/10.1016/j.ifacol.2018.06.127.
[32] Matušů R. Calculation of robustly stabilizing PI controllers for linear time-invariant systems with multiplicative uncertainty. In: Intelligent systems in cybernetics and automation control theory – Advances in intelligent systems and computing, Vol. 860. Cham: Springer Nature Switzerland AG; 2019, p. 259–63. http://dx.doi.org/10.1007/978-3-030-00184-1_24.
[33] Matušů R, Prokop R. Robustly stabilizing regions of PI controllers parameters for systems with additive uncertainty. In: Proceedings of the 29th DAAAM international symposium. Vienna, Austria; 2018, p. 176–9.
[34] Yaniv O. Design of low-order controllers satisfying sensitivity constraints for unstructured uncertain plants. Internat J Robust Nonlinear Control 2004;14(16):1359–70.
[35] Dúbravská M, Harsányi L. Control of uncertain systems. J Electr Eng 2007;58(4):228–31.
[36] Chokkadi S, Kumar SS. Design of robust controller for an uncertain system described by unstructured uncertainty model using small gain theorem. In: International conference on automation, computational and technology management. London, UK; 2019, p. 459–63.
[37] Emami T, Watkins JM. Robust performance characterization of PID controllers in the frequency domain. WSEAS Trans Syst Control 2009;4(5):232–42.
[38] Karšaiová M, Bakošová M, Vasičkaninová A. Robust control of a hydraulic system with unstructured uncertainties. In: Proceedings of the 18th international conference on process control. Slovakia: TatranskÁ Lomnica; 2011, p. 344–7.
[39] Keshtkar N, Röbenack K. Unstructured uncertainty based modeling and robust stability analysis of textile-reinforced composites with embedded shape memory alloys. Algorithms 2020;13(1). http://dx.doi.org/10.3390/a13010024.
[40] Matušů R, Şenol B, Pekař L. Robust PI control of interval plants with gain and phase margin specifications: Application to a continuous stirred tank reactor. IEEE Access 2020;8:145372–80.
[41] Gryazina EN, Polyak BT, Tremba AA. Design of the low-order controllers by the H_∞ criterion: A parametric approach. Autom Remote Control 2007;68:456–66.
[42] Garpinger O, Hägglund T, Åström KJ. Performance and robustness trade-offs in PID control. J Process Control 2014;24(5):568–77.
[43] Schlegel M, Medvecová P. Design of PI controllers: H_∞ region approach. In: IFAC-papersonline, 51, (6) Proceedings of the 15th IFAC conference on programmable devices and embedded systems. 2018, p. 13–7.
[44] Ho M-T, Huang S-T. Robust PID controller design for plants with structured and unstructured uncertainty. In: Proceedings of the 42nd IEEE international conference on decision and control. Maui, Hawaii, USA; 2003.
[45] Ho M-T, Huang S-T. On the synthesis of robust PID controllers for plants with structured and unstructured uncertainty. Internat J Robust Nonlinear Control 2005;15(6):269–85.
[46] Atsumi T, Messner WC. Modified bode plots for robust performance in SISO systems with structured and unstructured uncertainties. IEEE Trans Control Syst Technol 2012;20(2):356–68.
[47] da Silva de Aguiar RS, Apkarian P, Noll D. Structured robust control against mixed uncertainty. IEEE Trans Control Syst Technol 2018;26(5):1771–81. http://dx.doi.org/10.1109/TCST.2017.2723864.
[48] Shenton AT, Shafiei Z. Relative stability for control systems with adjustable parameters. J Guid Control Dyn 1994;17(2):304–10.
[49] Cavicehi TJ. Phase-root locus and relative stability. IEEE Control Syst Mag 1996;16(4):69–77.
[50] Barth EJ, Zhang J, Goldfarb M. Control design for relative stability in a PWM-controlled pneumatic system. J Dyn Syst Meas Control 2003;125(3):504–8.
[51] Tan N, Kaya I, Yeroglu C, Atherton DP. Computation of stabilizing PI and PID controllers using the stability boundary locus. Energy Convers Manage 2006;47(18–19):3045–58.
[52] Stojić MR, Vukosavić SN. A generaliztion of Kharitonov's four-polynomial concept for robust relative-stability problems. In: Facta universitatis, Series: Electronics and energetics, vol. 6, (no. 1):1993, p. 1–12.
[53] Dasgupta S, Fu M, Schwarz C. Robust relative stability of time-invariant and time-varying lattice filters. IEEE Trans Signal Process 1998;46(8):2088–100.
[54] Krutikova IR, Gaivoronsky SA. Application of the methods of root locus and D-decomposition for the analysis of the robust relative stability of the system. In: Proceedings of the 8th international scientific and practical conference of students, post-graduates and young scientists: Modern technique and technologies. Tomsk, Russia; 2002, p. 167–8.
[55] Karimi A. Robust control [online], presentation slides, laboratoire d'automatique, école polytechnique fédérale de lausanne. 2021, (Swiss Federal Institute of Technology in Lausanne), Switzerland, Available from URL: <https://www.epfl.ch/labs/la/wp-content/uploads/2018/08/robust.pdf>, [Accessed 09 September 2021].
[56] Burns RS. Advanced control engineering. Oxford, UK: Butterworth-Heinemann; 2001.
[57] Matušů R, Şenol B. Description and analysis of systems with unstructured additive uncertainty. In: Cybernetics approaches in intelligent systems: computational methods in systems and software 2017, Vol. 1. Advances in intelligent systems and computing, vol. 661, Cham, Switzerland: Springer International Publishing AG; 2018, p. 1–9. http://dx.doi.org/10.1007/978-3-319-67618-0_1.
[58] Smutný L, Škuta J, Farník J. Model teplovzdušného obvodu (model of hot-air circuit). Technical report to HS 311107 "Technická pomoc při návrhu a zhotovení modelu teplovzdušného obvodu (Technical assistance in the design and manufacture of a model of hot-air circuit), VSB, Czech Republic: Technical University of Ostrava; 2002, (In Czech).
[59] Matušů R. Robust control of systems with parametric uncertainty: An algebraic approach [Doctoral Thesis], Czech Republic: Faculty of Applied Informatics, Tomas Bata University in Zlín, Zlín; 2007.
[60] Matušů R, Prokop R, Vojtěšek J. Control of airflow speed in laboratory model of hot-air system with perturbed parameters. In: Proceedings of 16th international conference on process control. ŠtrbskÉ Pleso, Slovakia; 2007.
[61] Matušů R. Control of airflow speed in hot-air tunnel with uncertain parameters. In: Transactions of the VŠB – Technical University of Ostrava, Mechanical Series, LV (1), 2009, p. 181–8.
[62] Matušů R, Prokop R. Single-parameter tuning of PI controllers: Theory and application. J Franklin Inst B 2011;348(8):2059–71. http://dx.doi.org/10.1016/j.jfranklin.2011.05.021.
[63] Klán P, Honc D, Jindřich J. Nová měřicí jednotka CTRL V3 (new measuring unit CTRL V3). In: Proceedings of conference MATLAB 2003. Prague, Czech Republic; 2003, (In Czech).
[64] Dušek F, Honc D. Využití sériové linky pod matlabem verze 6 (use of serial link under MATLAB 6). In: Proceedings of conference MATLAB 2002. Prague, Czech Republic; 2002, (In Czech).